1

Research Background and Recent Progress of Perovskite Photovoltaics

Tsutomu Miyasaka[1,2] *and Ajay K. Jena*[1]

[1] *Toin University of Yokohama, Graduate School of Engineering, 1614 Kurogane-cho, Aoba-ku, Yokohama, Kanagawa 225-8503, Japan*
[2] *The University of Tokyo, Research Center for Advanced Science and Technology, 4-6-1 Komaba, Meguro-ku, Tokyo 153-8904, Japan*

1.1 Introduction

Perovskite solar cells (PSCs) are thin-film semiconductor-type solar cells that are similar to practical solar cells using compound semiconductors (GaAs, CdTe, etc.) and amorphous Si in photovoltaic (PV) industries. The advantage of these thin-film cells over the most popular crystalline Si solar cells is their processability into lightweight, thin, flexible devices. Lightweight and mechanical flexibility are significant added values sought for next-generation PV devices. Flexibility enables the device to be attached to curved surfaces of outdoor and indoor structures. Lightweight is particularly advantageous for mounting the device on mobile objects including cars and people. As a single-junction cell, GaAs achieves exceptionally high performance with a power conversion efficiency (PCE) (29%) exceeding the highest efficiency of crystalline Si cells (26%). However, high cost of GaAs semiconductor films based on their vacuum and high-temperature processes has limited its applications to small devices (transistors, lasers, etc.) or solar cells of space satellites. Among these thin-film solar cells, PV devices based on metal halide perovskite semiconductors were invented between 2006 and 2009 as an extension of the research on dye-sensitized solar cells (DSSCs) [1]. While having the advantage of a cost-efficient fabrication process, PSCs have evolved as the sole high-efficiency (>25%) solar cell type that can compete with the highest-efficiency Si cells [2]. Although perovskite materials have been generally known as metal oxides or chalcogenides, the composition of perovskites with superior PV functions is of a family of metal halide perovskites, which possess unique chemical and physical properties [3]. Unlike oxide perovskites, halide perovskites are highly ionic crystals characterized as ionic conductors. Here, perovskite crystals composed of lead (Pb) halide frameworks have good optical and physical properties suitable for photovoltaic conversion. Lead halide perovskites and their source materials for crystallization are soluble in polar solvents (alcohol, water, dimethylformamide,

Perovskite Photovoltaics and Optoelectronics: From Fundamentals to Advanced Applications,
First Edition. Edited by Tsutomu Miyasaka.

etc.). This makes it possible to apply the solution coating as a printing process for preparing thin crystalline films of perovskites as light absorbers. Owing to the strong light absorption property (high value of extinction coefficient $\sim 10^5\ cm^{-1}$) of halide perovskite semiconductors, PV cells can be designed with a thin film of light absorber (0.5–1 μm).

The basic structure of lead halide perovskite is $APbX_3$, in which A is a monovalence organic or inorganic cation. The halogen anion (X) is highly electronegative, enhancing the ionicity of the perovskite. Its type (I, Br, Cl) strongly affects the spectral absorption and bandgap of the material. The PV function of halide perovskites was first discovered with composition containing organic cations (A) instead of inorganic alkali cations [1, 3]. Composing of methylammonium (MA) cations and iodine as a halogen, $MAPbI_3$ exhibits excellent PV properties with a narrow bandgap (approximately 1.6 eV) absorbing the entire visible light up to 800 nm. Various lead halide perovskites have been synthesized by replacing MA and iodine with other organic groups and halides (Br and Cl), respectively. Here, halogen replacement enables continuous tuning of the bandgap due to the ratio of mixed halogens. Such halogen-dependent tunability of optical properties is similar to that of other metal halide-type ionic semiconductors. A typical example is Ag halide, which has been well investigated in photographic materials research. Ag halides are classified as n-type semiconductors with optical absorption at wavelengths less than 450 nm. Photogenerated free electrons that diffuse in a micrometer-sized grain of Ag halide crystal are eventually trapped by interstitial Ag^+ ions as the mechanism of latent image $(Ag(0)_n,\ n = 2–4)$ formation. Research on quantum sensitivity in latent image (Ag_4) formation revealed that photoexcited free electrons can transfer to form the latent image virtually without recombining with holes [4, 5]. Such efficient diffusion of free carriers in ionic crystals is possibly stabilized by the Coulombic screening of electrons and holes in the presence of cations and anions. The same effect is assumed to stabilize free electrons and holes in the halide perovskite ionic crystal and enables long-distance diffusion of the free carriers. Table 1.1 shows a comparison of the bandgaps obtained by exchanging halogens in halide perovskites $(MAPbI_{1-x}Br_x)$ and silver halides $(AgI_{1-x}Br_x)$. Here, the bandgap

Table 1.1 Comparison of optical properties of silver halide and lead halide perovskites.

Ionic semiconductor	Silver halides			Halide perovskites		
	AgCl	AgBr	AgI	$MAPbCl_3$	$MAPbBr_3$	$MAPbI_3$
Transition	direct (indirect)	direct (indirect)	direct	direct	direct	direct
Bandgap (eV)	5.2 (3.0–3.3)	4.3 (2.5–2.8)	2.8	2.9	2.35	1.55–1.60
Absorption edge (nm)	~240 (~390)	~290 (~470)	~440	~420	~520	~780
Semiconductor type	intrinsic, n	intrinsic	intrinsic, p	(intrinsic)	intrinsic	intrinsic

shifts to less energy (optical absorption edge to longer wavelength) in the order of $Cl \rightarrow Br \rightarrow I$. $MAPbI_3$, $MAPbBr_3$, and $MAPbCl_3$ exhibit bandgap energies of 1.60, 2.35, and 3.0 ± 0.1 eV, respectively [6]. In chemical crystallization, the ratio of mixed halides, such as the Br–I mixture, can be freely controlled in an attempt to continuously adjust the bandgap. Such synthetic flexibility of compositional design is a rare advantage of halide perovskite semiconductors.

The crystal of $MAPbI_3$ has an isotropic three-dimensional (3D) structure, which is beneficial for PV materials that must avoid anisotropic diffusion of photogenerated carriers. While 3D perovskites are suitable for PV applications, one-dimensional (1D) and two-dimensional (2D) structures of perovskites are synthesized by varying the size of the organic cation; their luminescent properties due to the photoexcited exciton and quantum confinement effects were studied earlier than those properties with PV applications. These dimensional variations of halide perovskite families are summarized in relation to their PV applications in Chapter 2. For perovskites of all dimensions, lead halide (PbI_2) that composes its inorganic part is a skeletal structure contributing to the conductivity and PV properties, while organic cations that modify the crystalline phase and lattice size affect the optical properties of the perovskite. Historically, it is known that PbI_2 itself is a photosensitive halide material that has been used to replace high-cost silver halides in photographic engineering [7]. While PbI_2 has a spectral sensitivity over 500 nm, the organic cation MA drastically enhances the sensitivity over the entire visible light region of up to 800 nm.

The progress of perovskite photovoltaics over the last 10 years has been remarkable. In 2005, our research group began the experiments to crystallize $MAPbI_3$ and $MAPbBr_3$ on a TiO_2 mesoporous layer as the visible light absorber and sensitizer of photoelectrochemical cells. Using $MAPbBr_3$ as a quantum dot-like nanocrystalline absorber on a TiO_2 electrode combined with an iodide-containing liquid electrolyte, a PCE of 2.2% was obtained in 2006 [8]. $MAPbI_3$ with a narrower bandgap increased the photocurrent density and improved the efficiency of up to 3.8%. This result was reported in the first publication showing a perovskite-based photovoltaic (PV) cell in 2009 [1]. In 2012, the efficiency of the $MAPbI_3$-based PV cell exceeded 10% when the thickness of the perovskite absorber on the solidification of the cell structure was increased [9]. After the efficiency boost, improvements made to the composition of perovskite and to the quality of charge transport materials resulted in a rapid increase in the power conversion efficiency (PCE) of PSCs, reaching the latest record of 25.5% [2], which is comparable with the top PCE of crystalline Si solar cells. Within 10 years, the PCE of PSCs achieved a greater than sixfold increase as the result of a considerable number of research groups, both in chemistry and physics, who have studied this new field of photovoltaics. Such rapid progress in the PCE development has not been observed for any other type of PV material and is unprecedented in the R&D of photovoltaics (PVs). Figure 1.1 shows the progress of PCE in the research of perovskite photovoltaics. Not only the high efficiency but also the low-cost solution-based processes for device fabrication testify to the immense potential of PSCs to lead the next generation of photovoltaics. Here, the advantages of halide perovskites are (i) intrinsically high efficiency in conversion between photonic and electronic quanta and energies, (ii) wavelength (bandgap)

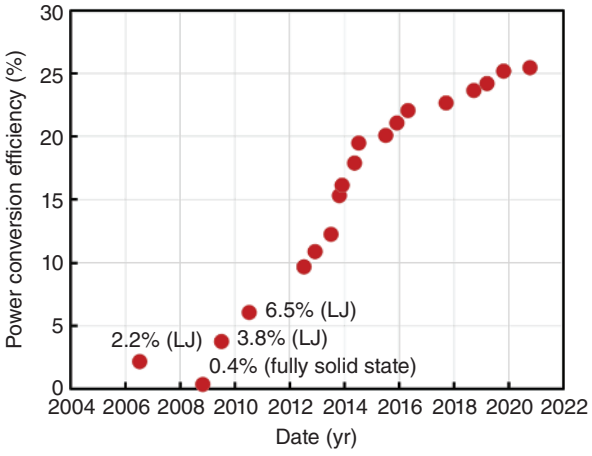

Figure 1.1 Progress of power conversion efficiency (PCE) of halide perovskite-based photovoltaic cells. LJ indicates liquid-junction photoelectrochemical cell in the early days of the research.

tunability based on changing the chemical composition of perovskite by chemical synthesis, (iii) thin (<1 μm) film of perovskite absorber as the active layer, and (iv) low cost of perovskite materials and printing processes in manufacture. There is no other photovoltaic device fulfilling all these aspects and enabling high device performance.

The highly interdisciplinary nature of the research enabled such rapid progress of PSCs. While solution-based crystallization of perovskite materials involves a great deal of knowledge and skill in chemistry, optical and electrical characterizations of solid-state crystals (semiconductors) are based on theories of physics. Because device development is achieved through a complete collaboration between chemistry and physics, the research field has gained interest from a large community of researchers worldwide [3, 10]. As a result of this interdisciplinary science, many applications beyond photovoltaics have been found for halide perovskites. Rare opto-physical properties of halide perovskites have stimulated the exploration of new functions in optoelectronics for these materials. One such function is high-performance light emitter. We observed intense green light emissions from spin-coated thin films of $MAPbBr_3$ under exposure to ambient air at room temperature [11]. Such efficient photoluminescence (PL) of perovskite films is a subject of intense study in fundamental science to assess defect-induced carrier recombination. At the same time, high PL performance leads to the fabrication of wavelength-tunable light-emitting diodes (LEDs) and perovskite-based lasers (see Chapter 12). Halide perovskites have many other applications in optoelectronics. They are represented in photodetectors, image-sensing devices, X-ray detectors, memory devices, etc. and their particular applications to optical detectors will be introduced in Chapters 13 and 14.

The fact that halide perovskite has excellent properties does not mean that perovskite photovoltaic and optoelectronic devices are ready for industrial use. One of the remaining important issues is ensuring high stability and durability of the perovskite and surrounding carrier-transporting materials. To overcome this, considerable efforts are being made in both fundamental research and engineering. In

fact, this is the main direction of ongoing research on perovskite-based devices. Furthermore, here, much effort is devoted to the discussion of this important issue. The intrinsic stability of halide perovskites is assumed to be due to the nature of their ionic migration, which is a characteristic of metal halide materials as soft ionic semiconductors. Such ionic conductivity is responsible for the peculiar behavior of carrier transport in the perovskites. For example, ionic migration is implicated as a main cause of the generation of hysteretic behavior in the current–voltage characteristics of the device. The structure of the crystal lattice can change by the partial exchange of ions during the storage of the device. Although ion migration is associated with the stability issue, it plays an important role in screening charges (positive and negative) against Coulombic (electrostatic) interactions to stabilize free carriers for long-range diffusion (>1 μm). Therefore, the question of how to control the behavior of mobile ions by compositional and morphological improvements has become the main focus of the study to solve the stability issue. Various methods have been attempted to improve the quality of perovskite devices for practical use. The purpose of this book is to introduce the fundamental chemical and physical properties of halide perovskite materials and their device characteristics in photovoltaic conversion when used with partner charge transport materials. In the following sections, we will introduce the background of the research on halide perovskite PV materials and outline ongoing methods to enhance the efficiency and stability of perovskite devices, challenges to achieving these goals, and strategies to overcome those challenges.

1.2 History of Halide Perovskite Photovoltaics

1.2.1 Discovery of the Perovskite Crystal Form

The research on perovskite materials dates back to 1839 when the Prussian mineralogist and crystallographer Gustav Rose determined its composition [12, 13]. The perovskite mineral was discovered in a piece of chlorite-rich skarn in the Ural Mountains of Russia by mineral collector August Alexander Kämmerer, who sent the sample to Gustav Rose in Germany for analysis. It was a black mineral (Figure 1.2a), and its composition was calcium titanate ($CaTiO_3$). Kämmerer requested that the new mineral be named in honor of the decorated Napoleonic Wars veteran Count Lev A. Perovskiy (1792–1856). Additional information as an interesting story on the discovery of perovskite and collaborations between Russian and German mineralogists has been published as an essay [15]. The crystal structure of perovskite, $CaTiO_3$, was studied in 1925 in Norway [13], following the first industrial patent of $CaTiO_3$ pigment by Victor M. Goldschmidt in 1922, who also conducted a crystal structure study and proposed the fundamental rule of the tolerance factor (see section 1.6.2) that indicates the stability and distortion of crystal structures [16]. Researches on these oxide perovskites have led to their industrial applications in electronic devices. The high dielectric constant discovered for $BaTiO_3$ [17] has, to date, led the industry of ferroelectrics such as capacitors, superconductors, piezoelectric devices, proton conductors, fuel cells, and memory storage devices. Although other metal oxide

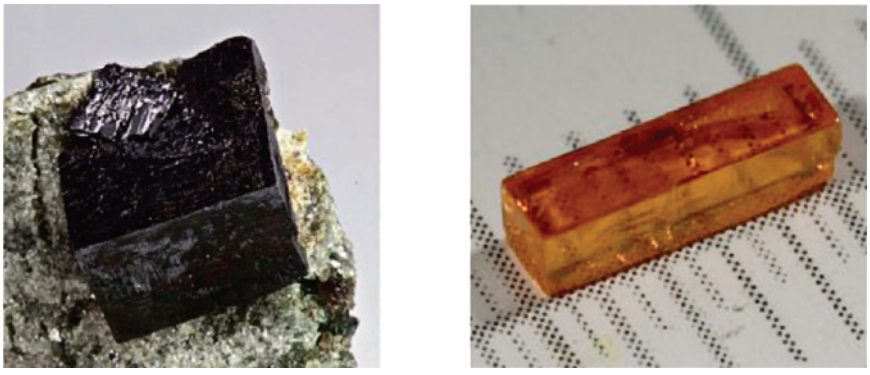

(a) (b)

Figure 1.2 Natural mineral of perovskite comprising $CsTiO_3$ (a) (image taken from http://www.geologypage) and a single crystal of lead halide perovskite, $CsPbBr_3$, synthesized by crystallization from solution (b) [14]. Source: Reprinted with permission from Dirin et al. [14]. Copyright 2016, American Chemical Society.

perovskites, such as $BaTiO_3$, $LiNbO_3$, $PbTiO_3$, $SrTiO_3$, $BiFeO_3$, etc., also work as ferroelectric ceramics, some of them, typically $BiFeO_3$, have been found to exhibit photovoltaic functions, known as ferroelectric photovoltaics [18]. However, these oxide perovskites have large bandgaps (>2.5 eV) that lack in light-harvesting ability and exhibit low efficiency in the collection of free charges. Therefore, oxide perovskites do not exhibit good semiconducting properties suitable for photovoltaic absorbers.

1.2.2 Discovery of Metal Halide Perovskites

Perovskite generally represents a type of crystal structure with the chemical formula ABX_3, where A and B are alkali and metal cations, respectively, and X is an anion (Figure 1.3). In an ideal cubic structure, the B cation has a sixfold

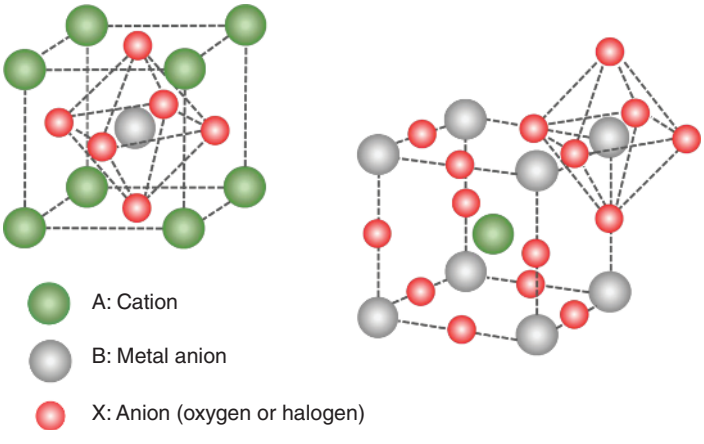

Figure 1.3 General crystal structure of perovskite, ABX_3 (X is oxygen or halogen).

configuration, surrounded by an octahedron of anions, and the A cation is in a 12-fold cuboctahedral configuration with coordination of 12 anions (Figure 1.3 right). The cubic unit cell of such compounds consists of A cations at the cube corner positions, B sitting at the body-center position, and X anions occupying the face-centered positions. Before halide perovskites attracted attention as photovoltaic semiconductors, perovskites were generally known as inorganic metal oxides (A = alkali cation, X = oxygen).

The class of halide perovskites differs from oxide perovskites in having halide anions in place of oxide anions (ABX_3; A = monovalent cation, B = divalent metal cation, X = halogen anion). As ionic crystals, halide perovskites have higher ionic crystallinity than oxide perovskites due to strong ionicity of halide anion. In halide perovskites, charge neutralization is established in the lattice structure by the coordination of a large number of cations and anions as mentioned above. Therefore, a slight structural strain due to fluctuations in the distance between ions (or ionic radius) and the coordination number leads to changes in the 3D structure of the crystal (see section 1.6.2). 3D halide perovskites demonstrate the semiconducting properties and strong visible light absorption desired for PV applications. The discovery of such halide perovskites dates back to the 1890s. In 1893, Wells conducted a comprehensive study on the synthesis of lead halide crystals from solutions including cesium (Cs)-based $CsPbX_3$ (X = Cl, Br, I) [19]. Figure 1.2b shows an orange crystal of $CsPbBr_3$. In 1957, Danish researcher Møller found that $CsPbCl_3$ and $CsPbBr_3$ have a perovskite structure [20, 21], showing a tetragonally distorted structure that undergoes transition to a pure cubic phase at high temperatures [21]. A simple solution process for the synthesis of these lead halide crystals might have inspired researchers to use other cations in place of Cs. Weber found that organic cation ($CH_3NH_3^+$) replaces Cs^+ to form $CH_3NH_3MX_3$ (M = Pb [22], Sn [23], X = I, Br) and reported the first crystallographic study on organic–inorganic hybrid lead halide perovskites. Toward the end of the last century, the synthesis of a large variety of halide perovskites composed of small and large organic cations was conducted by David Mitzi [24, 25]. Mitzi focused his studies on the physical properties of perovskite materials of low-dimensional structures such as 2D perovskites bearing a large organic group [25]. A comprehensive summary of this study will be introduced in Chapter 2. Based on this study, in the late 1990s, Professor Kohei Sanui was conducting a project through a Japanese national research program (JST–CREST). This project dealt with self-organized quantum confinement structures using the above perovskites and conducted a detailed investigation on the optical properties of 2D [26, 27] and 3D crystals [28, 29]. Although research paved the way to the applications of low-dimensional perovskite crystals to nonlinear optics and electroluminescence by utilizing sharp monochromatic optical absorption and luminescence [30, 31], at that time, it was not known that these materials could be employed for the utilization of solar energy. This requires a wide spectral absorption to harvest sunlight rather than having a sharp absorption and emission.

1.2.3 Beginning of Halide Perovskite Photovoltaics

The first and second generations of solar cells comprising silicon wafer-based and thin-film semiconductor-based solar cells, respectively, have improved markedly in terms of efficiency and stability. However, for silicon cells, ultrahigh purity of metallic silicon (>99.9999%), which can be obtained by the crystallization of melted Si in a furnace at more than 1400 °C, is an inevitable requirement for fabrication. Thus, the high process cost of wafer fabrication has prevented them to become the most popular alternative to fossil fuel-based energy sources such as thermal power generation (present cost is <US$ 0.1 per kWh of electric power). Therefore, in the search for cost-effective alternatives, there has been a great deal of research and development of third-generation photovoltaics, including organic PV cells (OPVs), DSSCs, and quantum dot (QD) solar cells. Although these cells could be processed very cheaply, their performances remained limited to a PCE of <15%, which apparently reduced the chances of their commercialization. During 2005–2006, while we continued our efforts toward further development of DSSCs [32–34], we explored the use of organic–inorganic lead halide perovskite as an absorber replacing the organic dye in DSSCs. What follows is a brief background on how perovskites began to be used for solar cells.

The research on perovskite-based photovoltaic devices started in 2005. This was the year after Miyasaka had established a venture company Peccell Technologies on the campus of Toin University of Yokohama (TUY), specializing in applications of DSSCs. In the same year, Akihiro Kojima, then a graduate student at Tokyo Polytechnic University (TPU), began to visit Miyasaka's laboratory to study DSSC through a collaboration between TPU and TUY. This collaboration was initiated by Dr. Kenjiro Teshima who was Kojima's mentor at TPU and later worked as a researcher in Peccell. The goal of the study was to examine the possibility of using lead halide perovskite as a sensitizer on mesoporous TiO_2 electrodes. It was also an extension of the study of Teshima and Kojima at TPU on the quantum photochemistry of halide perovskites. Teshima had served as a cooperating member of the JST-CREST national project (1997–2002) on self-organized quantum confinement structures using 2D perovskites [27, 28]. Therefore, Miyasaka's encounter with Teshima, who joined Peccell, was the impetus for the beginning of perovskite photovoltaics research. After initiating experiments using methylammonium lead halide perovskites as a DSSC sensitizer, we obtained preliminary results that demonstrated the visible light sensitization of TiO_2 with deposited nanocrystals of the perovskite. In October 2006, we presented our initial results at the Electrochemical Society's Annual Meeting in Mexico [8]. We continued this study, and Kojima joined our group as a doctoral course student at the Graduate School of University of Tokyo (UT), where Miyasaka served as a guest professor (2005–2010). Therefore, early perovskite studies from our team have been presented as a collaboration between three universities (TPU, TUY, and UT) and Peccell. Our perovskite photovoltaic cell first employed $CH_3NH_3PbX_3$ (X = I, Br) as a sensitizer on a TiO_2 mesoporous electrode used in conjunction with a lithium halide-containing electrolyte solution. Some of Kojima's initial works carried out before 2009 are presented in Figure 1.4.

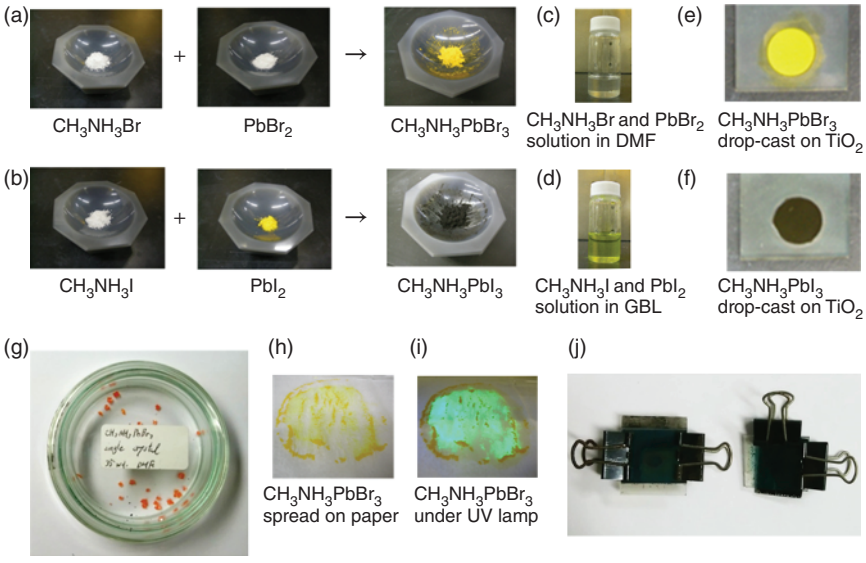

Figure 1.4 (a) and (b) show solid-state mixing routes for the synthesis of $CH_3NH_3PbBr_3$ and $CH_3NH_3PbI_3$, respectively. Solutions of (c) $CH_3NH_3PbBr_3$ and (d) $CH_3NH_3PbI_3$. Photographs of (e) $TiO_2/CH_3NH_3PbBr_3$ and (f) $TiO_2/CH_3NH_3PbI_3$ photoanodes. Photographs of (g) $CH_3NH_3PbBr_3$ single crystals, photographs of $CH_3NH_3PbBr_3$ powder spread on paper and exposed to (h) room light, (i) UV lamp (black light) showing strong emission under UV light, and (j) carbon-based perovskite photovoltaic devices as the first solid-state perovskite solar cell. Source: Reprinted with permission from Jena et al. [3]. Copyright 2019, American Chemical Society.

Assuming that the perovskite would function as a quantum dot-like sensitizer, the deposition of the perovskite was done by spin-coating the precursor solution, in which the loading amount of the perovskite was adjusted so as to obtain the thinnest layer of nanocrystalline perovskite covering a large surface area of a thick TiO_2 layer (~10 μm), similar to that of DSSC. This architecture was essentially different from the present PSC that uses a thin TiO_2 film (<0.1 μm) as an electron collector (or uses no mesoporous film). After optimizing the cell structure, we fabricated cells that yielded a PCE barely reaching 3.8%; this was published in the first peer-reviewed paper on perovskite-based photovoltaic cells in 2009 (Figure 1.5) [1]. Having also realized the necessity for a solid-state cell with a solid-state hole transport material (HTM), we attempted to prepare devices by employing a carbon/conductive polymer composite, obtaining a low PCE value (<1%). This was the first example of a full-solid-state perovskite photovoltaic cell, which we reported in an international conference (ECS) in 2008 [35, 36]. We later realized that such poor performance was apparently due to the significantly low loading amount of perovskite. This was also confirmed by Nam Gyu Park and coworkers, who improved our method to obtain a higher PCE by simply increasing the perovskite loading [37].

In 2011, we started a collaborative work with Henry Snaith (H. S.) of Oxford University for creating solid-state perovskite cells. This opportunity was arranged by Dr. Takurou Murakami (presently in AIST, Japan), who had joined the EPFL (Swiss

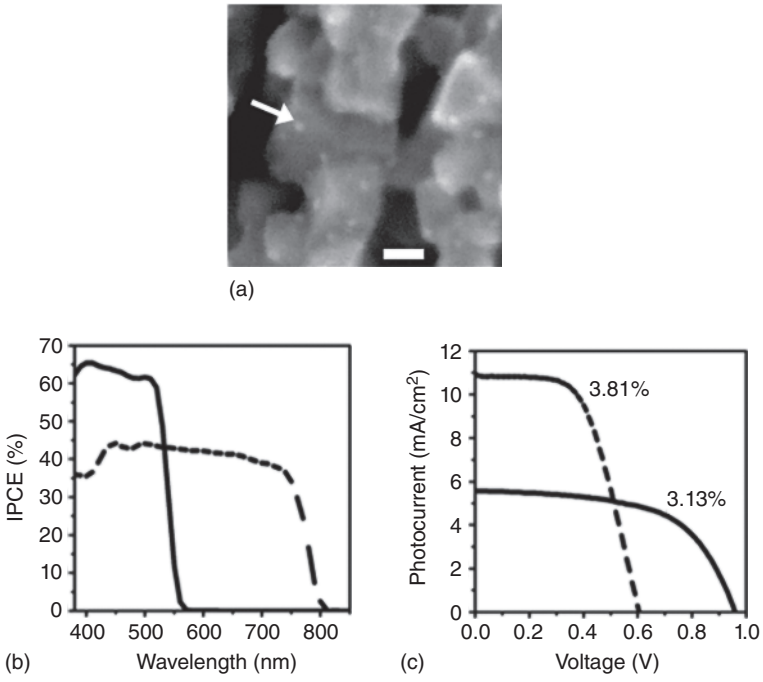

Figure 1.5 (a) SEM image (scale bar: 10 nm) of particles (shown by an arrow) of nanocrystalline $CH_3NH_3PbBr_3$ ($MAPbBr_3$) deposited on the TiO_2 surface. (b) incident photon to current conversion efficiency (IPCE) action spectra for photoelectrochemical cells using $MAPbBr_3/TiO_2$ (solid line) and $MAPbI_3/TiO_2$ (dashed line) photoanodes with a liquid electrolyte, 0.4 M LiBr and 0.04 M Br_2 dissolved in acetonitrile for the former and 0.15 M LiI and 0.075 M I_2 dissolved in methoxyacetonitrile for the latter photoanode. (c) Photocurrent–voltage characteristics for cells using $MAPbBr_3/TiO_2$ (solid line, PCE = 3.13%) and $MAPbI_3/TiO_2$ (dashed line, PCE = 3.81%) under 100 mW/cm^2, air mass (AM) 1.5 irradiation. Source: Reproduced with permission from Kojima et al. [1]. Copyright 2009, American Chemical Society.

Federal Institute of Technology in Lausanne) [38], where H. S. was also a researcher, to continue his research on DSSC after having finished his PhD in 2005 under the supervision of Miyasaka at TUY. In 2009, Dr. Murakami started a Japan Society for Promotion of Science (JSPS) international collaboration project on the DSSC study, and fabrication of perovskite-based PV cells was planned as an extension of this project. In 2011, Michael Lee, a PhD student of the H. S. group in Oxford, spent several months in our group to learn the method of preparing the perovskite. Because H. S. had worked on solid-state DSSCs using an HTM [39], our aim was to solidify the perovskite-sensitized cell with a spin-coated layer of an organic HTM, spiro-OMeTAD (2,2′,7,7′-tetrakis(*N,N*-dimethoxyphenylamine)-9,9′-spirobifluorene). However, we immediately faced difficulty in stabilizing perovskite crystals against dissolution into the solvent used in the spiro-OMeTAD solution. We later found a way to suppress the dissolution of perovskite by mixing chloride with the composition of perovskite, $MAPbI_{3-x}Cl_x$, which eventually produced cells with a PCE of 10.9% [9]. Here, the device using an insulating mesoporous Al_2O_3 as a

scaffold for $MAPbI_3$ crystals exhibited a higher voltage and PCE than those using TiO_2 as scaffold. Indeed, it was an indication of the long diffusion length of carriers in perovskite, which was also indicative from our observation of intense green light photoluminescence (PL) from bromide perovskite ($MAPbBr_3$) spread on paper (see Figure 1.4h, i) and coated on mesoporous Al_2O_3 [11]. The long carrier diffusion length of the lead halide perovskite, which has been later confirmed by opto-physical analysis [40, 41] and carrier mobility [42] characterizations, has brought radical changes in our understanding of the functioning of PSCs, distinguishing the new technology from any other organic and hybrid material-based solar cells. PSCs grew larger and shone brighter in the shortest time measured in the history of PV technology. A considerable number of studies, both in chemistry and physics, have been conducted toward improving the quality of solution-processed perovskite crystalline films and their heterojunction interfaces by reducing the defect density at grain boundaries and interfaces. These great efforts have led to the realization of high PCEs of over 25% [43, 44] and current record PCE of 25.5% [2].

1.3 Semiconductor Properties of Organo-Lead Halide Perovskites

The solid-state physics of halide perovskite semiconductors has been investigated in detail regarding their semiconducting properties, carrier transport mechanisms, and theories of defect-related charge recombination. PV applications have been mainly focused on 3D perovskite materials that perform isotropic carrier transport advantageous for power generation. Unlike conventional semiconductors, halide perovskites are ionic crystals. Their strongly ionic nature is due to the halide anion, which has a large negative charge. Ionic migration in halide perovskite materials is responsible for the unique behaviors of perovskite-based PV devices, including slow response and hysteresis in the current–voltage performance and instability of the material [45]. This will be discussed further in Sections 1.6.1 and 1.6.2. As an advantage in optical engineering, the semiconducting nature of halide perovskites allows the easy tuning of the bandgap and optical absorption by varying the halide ions. Figure 1.6 shows the wavelength tuning for the I and Br mixture of MA lead halide ($CH_3NH_3Pb(Br_xI_{1-x})_{3-y}Cl_y$, $0 \le x \le 1$) [46] and formamidinium (FA) lead halide ($HC(NH_2)_2PbBr_{1-y}I_y$, $y = 0$–1) [47]. The absorption edge wavelength corresponding to the bandgap energy changes proportionally with the content of bromide. When iodide is added to the perovskite structure, $FAPbBr_{1-y}I_y$ (Figure 1.6e) exhibits a continuous redshift from the edge wavelength of ~550 nm for pure bromide ($FAPbBr_3$) to ~830 nm for pure iodide ($FAPbI_3$). A constant emission peak shift similar to that of the absorption is also observed in the PL spectrum. These optical properties corroborate that mixed-halide perovskites can form good solid solutions as ionic crystals.

Strong bandgap absorption at the edge wavelength and broad flat absorption covering visible light wavelengths indicate that halide perovskites work as excellent absorbers for sunlight. MA lead iodide ($MAPbI_3$), which is a standard perovskite

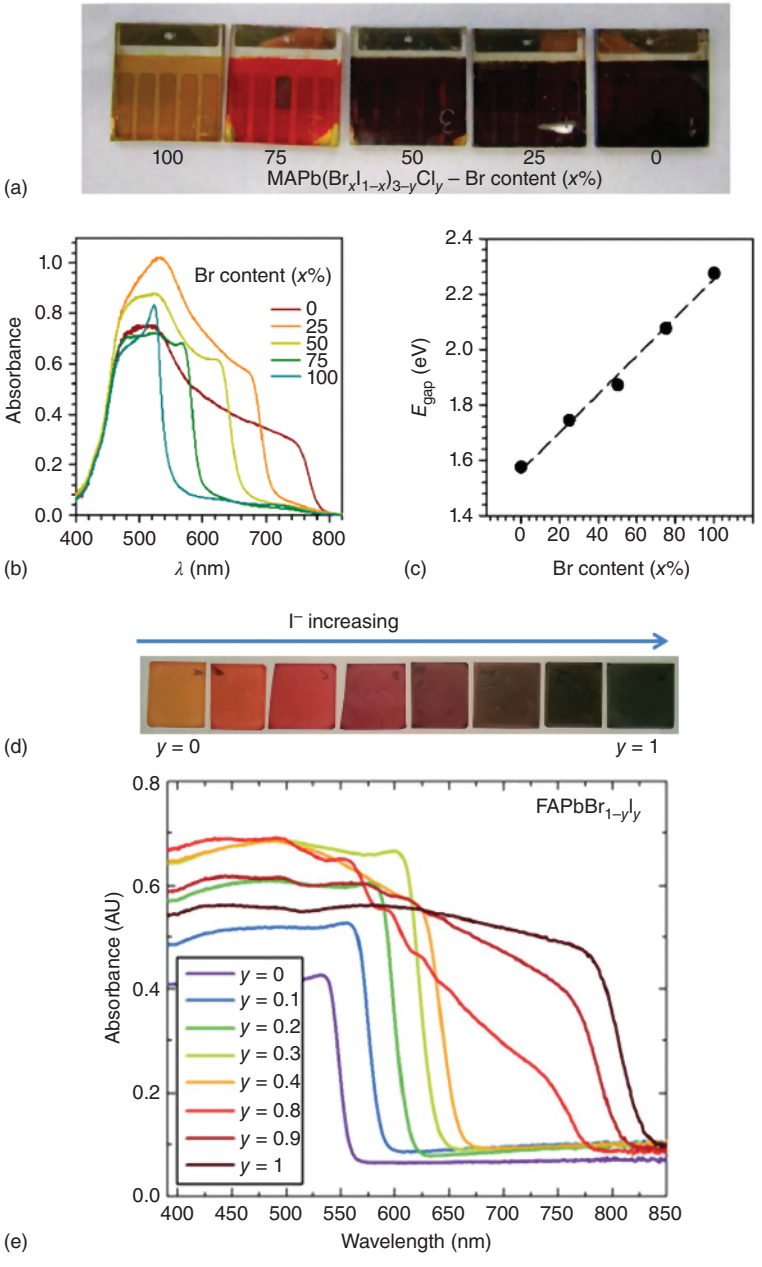

Figure 1.6 (a) Picture of perovskite devices bearing MA lead bromo-iodide perovskite, $CH_3NH_3Pb(Br_xI_{1-x})_{3-y}Cl_y$, ($0 \leq x \leq 1$), films with different Br/I molar ratios on mesoporous TiO_2 substrates. (b) Absorption spectra of the perovskites films and (c) their bandgap energies. Source: (a) Reprinted with permission from Suarez et al. [46]. Copyright 2015 American Chemical Society, (b, c) Suarez et al. [46]. (d) Photographs of FA lead bromo-iodide perovskite, $HC(NH_2)_2PbBr_{1-y}I_y$, films with y increasing from 0 to 1 (left to right) and (e) their absorption spectra. Source: (d) Reprinted with permission from Eperon et al. [47]. Copyright 2014 Royal Society of Chemistry, (e) Eperon et al. [47].

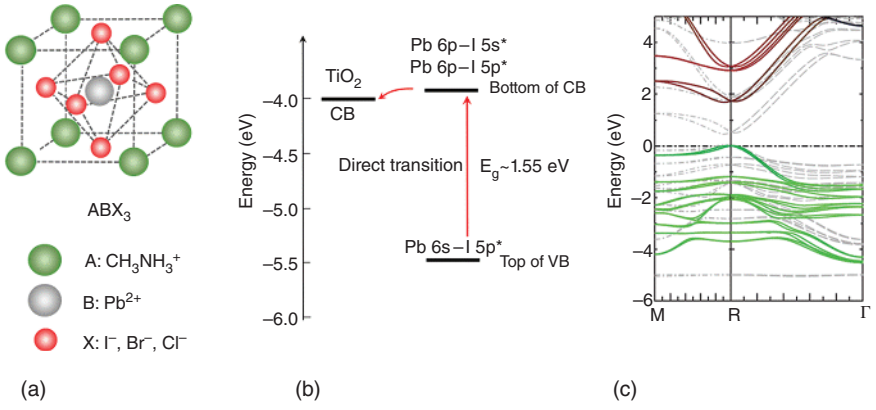

Figure 1.7 (a) Structure of organo-metal halide perovskite crystal. (b) Bandgap structure and energy levels of $MAPbI_3$ in relation to CB of TiO_2 as electron transport material (c) Electronic structure of $MAPbI_3$ based on the quasiparticle self-consistent GW approximation. Zero denotes the valence band maximum. Green and red solid lines depict bands of I 5p and Pb 6p, respectively, and light-gray dashed lines show corresponding bands in local-density approximation (LDA). Points denoted M and R are zone-boundary points. Source: Brivio et al. [49] and Miyasaka [10].

absorber in PV cells, can be characterized as a rare intrinsic semiconductor [48] exhibiting the excellent mobility of both photogenerated electrons and holes. Density functional theory (DFT) and first-principles theory-based calculations have corroborated the superior photophysical properties of $MAPbI_3$, which has long diffusion lengths for free carriers [40, 42]. Figure 1.7 shows the lattice structure of MA halide perovskite, $MAPbX_3$ (X = I, Br, Cl), and the band structures of $MAPbI_3$ based on studies by Kondo and coworkers [50] and Brivio et al. [49]. A characteristic feature of the electronic structure of $MAPbI_3$ is that both conduction band (CB) and valence band (VB) consist of antibonding orbitals as depicted in Fig. 1.7b. VB of $MAPbI_3$ consists of approximately 70% of I 5p orbitals and 25% of Pb $6s^2$ orbital (lone pair), while CB consists of a mixture of Pb 6p and other orbitals. Here, VB orbitals have a strong coupling between Pb lone-pair $6s^2$ and I 5p orbitals [51]. This structure is opposite to that of GaAs, in which VB and CB are formed by p and s orbitals, respectively.

The high symmetry and direct bandgap of $MAPbI_3$ and the p–p electronic transitions from VB to CB, enabled by the Pb s orbital lone pair, contribute to the high optical absorption coefficients of this material ($10^5\ cm^{-1}$) [52]. The unique defect properties of perovskite are attributed to strong Pb s–I p antibonding coupling, weak Pb p–I p antibonding coupling, and ionic characteristics [51]. Weak antibonding coupling between Pb p and I p orbitals fixes the conduction band minimum (CBM) close to the Pb p orbital, while strong Pb s–I p antibonding coupling lowers the valence band maximum (VBM) close to the I p orbital. Therefore, for vacancies (defects) formed by the removal of I^-, the defect state lies between the Pb p atomic orbital level and the CBM level, and for Pb^{2+} vacancies, the defect state is formed between I p and VBM levels. Hence, unlike other ionic semiconductors

where localized nonbonding orbitals surrounding the ion vacancies form trap states deep within the bandgap, such defects in perovskites ($MAPbI_3$) generate trap states that either reside within the bands (VB or CB) or exist as shallow traps near CB and VB. Carriers trapped in shallow defects can be easily detrapped and contribute to current generation. This explains the rare nature of perovskite semiconductors attributed with "defect tolerance". The defect-tolerant nature of perovskite is reflected by large carrier diffusion lengths as measured by PL lifetime, which are in the range of 1 μm (polycrystalline film) [40] to over 100 μm (single crystal) [42]. Furthermore, as $MAPbI_3$ is an intrinsic semiconductor, the mobility of its carriers is ambipolar, exhibiting a similar effective mass for both electrons and holes (0.23–0.29) [53]. Similar to inorganic photovoltaic semiconductors such as Si and GaAs, photogenerated carriers in $MAPbI_3$ behave as free carriers and can migrate without recombination for as long as several hundreds of nanoseconds, as shown in PL measurements [40, 54, 55]. It is also considered that the high ionic density in halide perovskites helps to suppress charge recombination by a charge-screening effect against Coulombic (electrostatic) interactions.

In summary, the important factors that support the superior performance and high efficiency of perovskite solar cells (PSCs) are (i) high optical absorption coefficient ($10^5\ cm^{-1}$) that allows the use of thin films (<0.5 μm), (ii) long carrier diffusion length and suppressed recombination (defect tolerance), and (iii) well-balanced charge transfer. In PV applications, the defect-tolerant nature of halide perovskite is especially important and leads to the generation of high voltage. The high PCE of PSCs is a result of high photovoltage (1.1–1.2 V) output rather than the amplitude of the photocurrent. The open-circuit voltage (V_{OC}) of all types of existing solar cells undergoes a large thermal loss from its bandgap energy. Such a voltage loss (V_{OC} deficit) often constitutes more than one-third of the bandgap energy (E_g). For example, Si p/n junction cells (E_g~1.1 eV, $V_{OC} \sim 0.7$ V), which are highly sensitive to small concentrations of impurity defects, show a significant reduction in V_{OC}, especially under operation at low incident light. In contrast, PSCs can generate a V_{OC} of over 1.2 V (1.26 V obtainable with $MAPbI_3$ [56]) with respect to their E_g of 1.55–1.6 eV. Figure 1.8 shows the average values of the V_{OC} deficit ($E_g/e - V_{OC}$) for different types of solar cells. The lowest value of the deficit is obtained for a single crystal of GaAs that, as a single-junction solar cell, is known to present the highest PCE value of 27.8%, exceeding the top PCE of crystal silicon (26.1%). With an E_g of 1.42 eV, the GaAs cell is capable of generating V_{OC} values up to 1.12 V. The small deficit of 0.3 eV is close to the Shockley–Queisser (SQ) theoretical limit [57, 58]. Semiconductors of perovskites and their solar cells are also superior in reducing the V_{OC} deficit to the range of 0.35–0.45 V. Detailed explanations and the determination of V_{OC} deficits will be provided in Chapter 5.

There is still a substantial loss in V_{OC}. One property related to the loss of efficiency that is still limiting the V_{OC} and efficiency of PSCs is the defect (trap) density in halide perovskite crystals, which is estimated to be from $10^{10}\ cm^{-3}$ (single crystals) [42, 59] to $10^{16}\ cm^{-3}$ (polycrystals) [55, 60]. This indicates that the purity of solution-processed polycrystalline films can be an important factor in minimizing defect and trap concentrations and thus further improving the efficiency. Equally

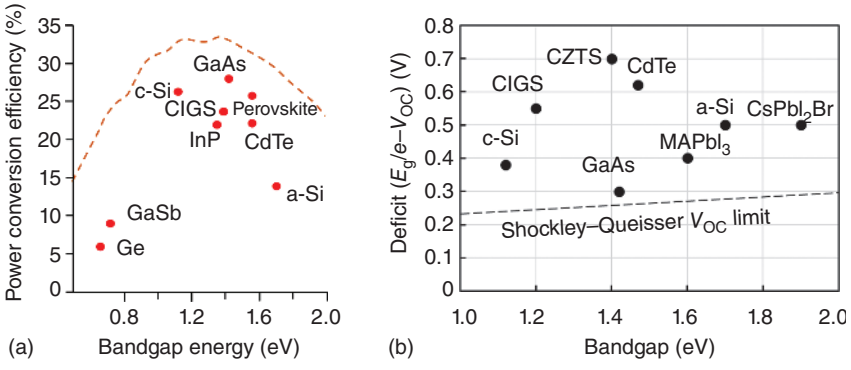

Figure 1.8 Power conversion efficiencies of solar cell as a function of bandgap energy (a) with Shockley–Queisser limit values in dotted line. Average values of V_{OC} deficit ($E_g/e - V_{OC}$) for different types of solar cells (b).

important are the losses caused by carrier recombination at heterojunction interfaces with electron and hole transport layers. Hence, understanding the function of PSCs in standard architectures and the use of optimized electron and hole transport layers are important for further performance improvement.

1.4 Working Principle of Perovskite Photovoltaics

Although mesoporous metal oxides such as TiO_2 and Al_2O_3 serve as a scaffold for holding perovskite nanocrystals, the perovskite PV device can work even without a mesoporous scaffold layer (planar heterojunction with compact TiO_2 layer for collecting electrons). This provides sufficient grounds for differentiating the PSC from the mechanism of sensitization and makes it clear that the PSCs work more like solid-state p–n junction solar cells in which perovskite functions as an intrinsic semiconductor (i) sandwiched between two selective (p and n) contacts. In the n–i–p structure, TiO_2 works as an n-type electron transport material (ETM), and a hole transport material (HTM) such as spiro-OMeTAD works as a p-type contact. Here, a typical device structure using transparent conductive electrodes such as F-doped tin oxide (FTO) or indium tin oxide (ITO) comprises a junction of FTO(ITO)/TiO_2/perovskite/spiro-OMeTAD/metal. In a p–i–n-type structure, which is otherwise known as an inverted structure, perovskite is sandwiched by a p-type material (e.g. conductive polymers such as poly(3,4-ethylenedioxythiophene [PEDOT-PSS]) at the bottom and an n-type layer (e.g. fullerene derivative such as [6,6]-Phenyl-C61 butyric acid methyl ester [PCBM]) at the top, forming a junction of FTO(ITO)/PEDOT-PSS/perovskite/PCBM/metal. Some typical architectures of PSCs are illustrated in Figure 1.9. The perovskite absorbs light to generate electrons and holes. Moreover, the electrons are selectively collected by the n-type ETM layer, while the holes are collected by the p-type HTM layer. Electrons flow through the external circuit to reach the p-type layer to combine with the holes. Figure 1.10

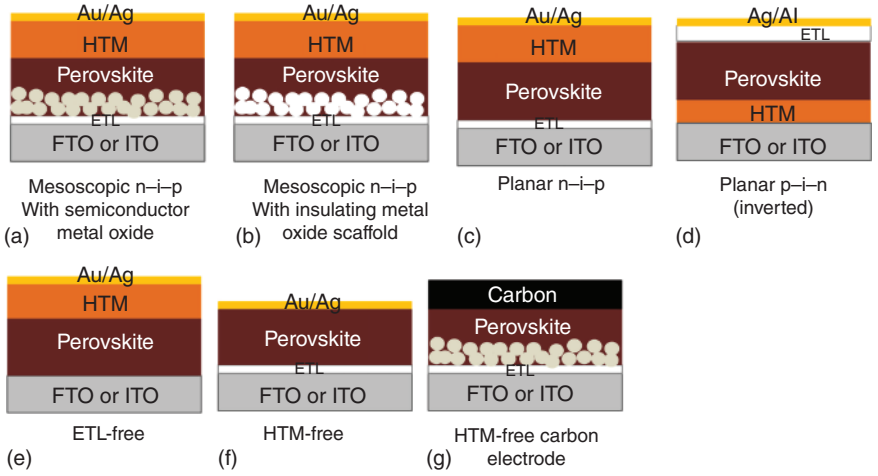

Figure 1.9 Variety of layered architectures for perovskite solar cells. Source: Jena et al. [3].

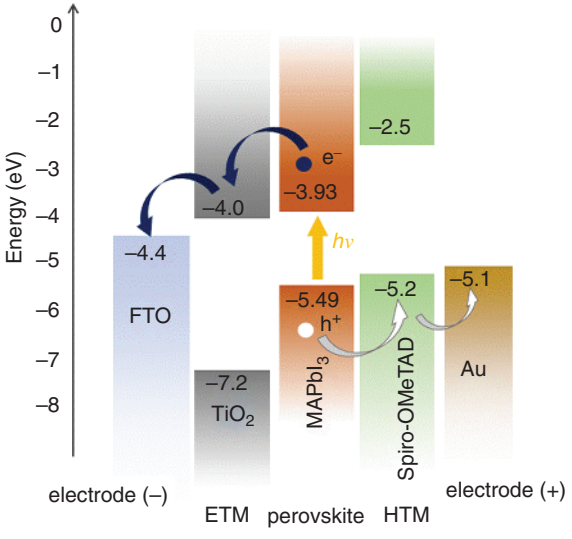

Figure 1.10 Energy diagram of a typical perovskite solar cell using $MAPbI_3$ as the perovskite absorber, TiO_2 as the ETM, and spiro-OMeTAD as the HTM. FTO and Au are front and back contacts.

shows the band diagram of a typical metal oxide ETM-based perovskite device (FTO/TiO_2/perovskite/spiro-OMTAD/Au).

An important factor that leads to the high PCE of PSCs is the open-circuit voltage (V_{OC}). The V_{OC} of some perovskite cells (1.18–1.26 V) [56, 61–63] approaches the SQ theoretical limit of V_{OC} (~1.32 V) based on the bandgap of the perovskite semiconductors (1.6 eV for $MAPbI_3$) [63, 64]. In PV cells, V_{OC} is generally determined by the energy gap between the Fermi levels of selective contacts, namely, p-type and n-type conductive layers. For the typical junction structure in Figure 1.10, these contacts are given by spiro-OMeTAD as the HTM and by TiO_2 as the ETM. Their energy gap corresponds to the difference between the highest occupied molecular orbital (HOMO) level of HTM and the CB level of TiO_2. Although FTO and

Au as conductive electrodes have their own work functions, their energy gaps have little influence on V_{OC} because of their low charge selectivity. Furthermore, the CB level of the TiO_2 ETM (–4.0 – –4.2 eV) tends to have less of an effect on controlling the energy gap that determines the maximum value of V_{OC}. This tendency is apparent when TiO_2 is replaced with SnO_2. Despite the low CB level of SnO_2 (approximately 0.25 eV lower than that of TiO_2), comparably high V_{OC} (>1.0 V) can be obtained using both ETMs [65, 66]. This fact may indicate that mesoporous metal oxides (TiO_2 and SnO_2) mainly function as scaffolds for perovskite crystals, and the material that primarily serves as an ETM is a thin compact oxide layer (general thickness < 10 nm) covering the surface of the FTO below the mesoporous layer. However, such a compact layer is considered to be too thin to exhibit the semiconductor property although it is capable of rectifying electron transfer at the interface by blocking hole injection. As a result, the energy gap that relates to the value of V_{OC} is assumed to be the difference between the CB level of the perovskite absorber and the HOMO level of the HTM. In fact, a high V_{OC} exceeding 1.1 V has been obtained with many perovskite devices using TiO_2 ETM with spiro-OMeTAD [61, 62, 66, 67]. Furthermore, some of the highest V_{OC} values of perovskite PV cells have been recently obtained by our group using SnO_2 ETMs. An SnO_2-based device using a multi-cation mixed-halide perovskite, $(CsFAMA)Pb(I,Br)_3$, and dithiophene-type HTM exhibited a V_{OC} of 1.19 V with a PCE of 22% [68]. Another SnO_2-based device using an all-inorganic perovskite, $CsPbI_2Br$, and a thiophene-type copolymer HTM achieved a high V_{OC} of over 1.4 V with a PCE of over 15.5% [69].

The small thermal loss from the bandgap of perovskites in V_{OC} generation reflects the superior semiconductor properties of halide perovskites such as ultralong carrier diffusion length [40, 52, 70], long carrier lifetime [71, 72], moderate carrier mobility [41, 73, 74], and high defect tolerance, all of which indicate an efficient suppression of carrier recombination [74]. Theoretical modeling of the electronic structures of $MAPbI_3$ shows that the defect formation influencing carrier recombination is limited to energetically shallow positions near the CB and VB levels rather than deep defects in the bandgap that strongly trap carriers. Material simulation based on first-principles theory suggests that such a superior structure is unique to lead iodide-based compositions [51] and is difficult to realize for other metal halide semiconductors (see Chapter 4 for more discussion of this topic). At the time of this review, the only non-lead halide perovskites able to increase PCE beyond 10% are tin (Sn)-based perovskites, which have electronic structures similar to lead halide perovskites and absorb visible light and near-infrared light. The latest progress of Sn perovskites will be described in Chapter 10. Unlike the single crystals of perovskite, solution-processed thin films of perovskites are composed of aggregates of nanocrystalline perovskite particles with dispersed grain size; the large number of defects formed on the grain surface and boundaries substantially influences the PV properties (see Chapter 3 for related topics). Hence, it is essential to minimize the defect density at the grain surface and boundaries by chemically modifying the molecular structure of perovskite at the contact interface. Chemical engineering for this purpose, such as increasing the grain size (decreasing the boundary area), improving the uniformity of film morphology, and passivating the defects using additives, not

only enhances the PV performance but also improves the stability of the perovskite films. Recent studies on perovskite photovoltaics have made considerable efforts to improve the quality of interfacial structures to ensure high stability of devices for industrial applications.

1.5 Compositional Engineering for the Halide Perovskite Absorbers

Flexibility to change the crystal composition by solution-based synthesis is a rare advantage of halide perovskite semiconductors. Replacing the A-site cation and the B-site anion with different organic or inorganic cations and halogen anions, respectively, has not only exerted a strong influence on the optical properties and PV efficiency of perovskite but also can increase its stability. A certain mix of cations at the A-site and halides at the B-site demonstrated superiority over single-cation/halide perovskites in terms of both efficiency and stability. Indeed, all the cells published in the NREL chart of record efficiency [2], except for the first entry for $MAPbI_3$, comprise a mix of cations, anions, or both. The most popular organic cation MA has the issue of thermal stability owing to the physical evaporation of this small molecule at temperatures above 120 °C [75]. In this aspect, the current high-stability development of perovskite PV cells tends to choose MA-free compositions [76] and/or all inorganic compositions [77]. Based on the ionic size and geometrical tolerance factor (τ), which is an empirical index widely used for predicting perovskite crystal structure (see Section 6.2), combinations of different cations such as MA, FA, Cs, Rb, and anions (I, Br, Cl) have been explored. Table 1.2 provides a list of A-, B-, and X-site ions and their sizes that are, or can be, used in certain combinations to form perovskite structures. Out of all possible combinations [79], the mixed perovskite that became the most popular in recent years is $(MA/FA/Cs)Pb(I/Br)_3$, which is known as triple-cation perovskite. The quadruple-cation perovskite, which includes Rb (i.e. $(MA/FA/Cs/Rb)\ Pb(I/Br)_3$) as the fourth cation, has also gained interest owing to its high cell efficiency and stability (see Chapter 8 for device performances of triple and quadruple-cation perovskites). For Rb-doped perovskites, it is assumed that Rb is localized in grain boundaries rather than in any lattice sites [80, 81].

According to DFT calculations, the cations in the A-site are considered to not contribute directly to the band structure. However, they play a significant role in providing structural stability of the crystal by charge compensation within the PbI_6 octahedra, largely based on their electrostatic (van der Waals) interactions [82] with the inorganic cage. Nevertheless, the size of the A-site cation can contribute either to the contraction or to the expansion of the crystal lattice, thereby altering the optical properties of the perovskite. Small inorganic cations such as Cs and Rb are expected to contract the lattice and thus increase the bandgap energy (E_g), while large organic cations such as FA^+ expand the lattice and decrease the E_g. FA^+, having a larger ionic radius ($r = 0.253$ nm) than MA^+ ($r = 0.217$ nm), expands the crystal a small amount, resulting in the decreased Pb—I bond distance, which eventually lowers E_g. Pure $FAPbI_3$ shows an E_g of 1.47 eV while the E_g for pure $MAPbI_3$ is

Table 1.2 Ionic radii of some of common A-site cations, B-site cations, and X-site anions used in hybrid perovskites.

Cations (A-site)	Effective ionic radius (pm)	Metal cation (B-site)	Effective ionic radius (pm)	Halogen anion (X-site)	Effective ionic radius (pm)
NH_4^+	146	Pb^{2+}	119	F^-	129
Methylammonium, $[CH_3NH_3]^+$, (MA)	217	Sn^{2+}	110	Cl^-	181
Formamidinium, $[CH(NH_2)_2]^+$, (FA)	253	Ge^{2+}	73	Br^-	196
Hydrazinium, $[NH_3NH_2]^+$	217	Mg^{2+}	72	I^-	220
Azetidinium, $[(CH_2)_3NH_2]^+$	250	Ca^{2+}	100		
Hydroxylammonium, $[NH_3OH]^+$	216	Sr^{2+}	118		
Imidazolium, $[C_3N_2H_5]^+$	258	Ba^{2+}	135		
Ethylammonium, $[(CH_3CH_2)NH_3]^+$	274	Cu^{2+}	73		
Dimethylammonium, $[(CH_3)_2NH_2]^+$	272	Fe^{2+}	78		
Guanidinium, $[(NH_2)_3C]^+$	278	Pd^{2+}	86		
Tetramethylammonium, $[(CH_3)_4N]^+$	292	Eu^{2+}	117		
Thiazolium, $[C_3H_4NS]^+$	320	Bi^{3+}	103		
3-Pyrrolinium, $[NC_4H_8]^+$	272	Sb^{3+}	76		
Tropylium, $[C_7H_7]^+$	333				
K^+	164				
Rb^+	172				
Cs^+	188				

Source: Hoefler et al. [78]. Licensed under CC BY-4.0.

1.55–1.60 eV. With an extended absorption edge (>800 nm), $FAPbI_3$ cells show a larger short-circuit photocurrent density (J_{sc}) that leads to a PCE value of over 20% [83]. MA and FA affect the intrinsic stability of perovskites. $MAPbI_3$ is fairly stable in its crystal structure at temperatures below 120 °C. However, $FAPbI_3$ readily crystallizes into a photoinactive phase (δ-$FAPbI_3$) at room temperature while this phase is transformed to the photoactive black phase (α-$FAPbI_3$) at high temperatures (125–165 °C) [84]. Such phase instability often affects the PV characteristics by reducing the fill factor (FF) of current density–voltage (J–V) curves. This can be overcome by a partial substitution of FA with MA. The incorporation of an MA^+, which has a dipole moment almost 10 times greater than that of FA^+, exhibits a stronger interaction with the PbI_6^{4-} octahedra, thus stabilizing the 3D arrangement of α-$FAPbI_3$ [85]. Despite the phase instability, the thermal stability of $FAPbI_3$ is significantly greater than that of $MAPbI_3$ [75]. $FAPbI_3$, when heated at 150 °C

for hours, does not change color, whereas $MAPbI_3$ becomes yellow (due to formation of PbI_2) at 150 °C (or even lower) for just 30 minutes [47]. Such thermal stability is attributable to the increased tolerance factor and stronger interaction of FA with iodide ions. The partial replacement of MA with FA also significantly improves the thermal stability of $MAPbI_3$. However, the FA inclusion strategy falls short of long-term durability because it is unfortunately more hygroscopic than MA and thus shows greater vulnerability to humidity [86]. Therefore, the incorporation of inorganic cation Cs has become an alternative. As reported by Niu et al. [87], approximately 9 mol% of Cs in $Cs_xMA_{1-x}PbI_3$ ($x = 0.09$) showed better PV performance (PCE of 18.1%) and thermal stability (at 120 °C for three hours) than pristine $MAPbI_3$ (PCE of 15.8%), while higher concentrations show surprisingly reduced stability. Cs inclusion can also stabilize $FAPbI_3$. Small and large tolerance factors, respectively, for $CsPbI_3$ ($\tau = 0.85$) and $FAPbI_3$ ($\tau = 0.98$) stabilize the perovskites in orthorhombic and hexagonal structures, respectively, both of which exhibit pale yellow color due to the formation of PbI_2 and not photovoltaically active. However, an effective tolerance factor can be tuned to form a cubic structure ($0.9 \leq \tau \geq 1$) by alloying $CsPbI_3$ with $FAPbI_3$ ($FA_xCs_{1-x}PbI_3$), and the cell performance of $FAPbI_3$ improves with 10–20% mixing of Cs. For example, $FAPbI_3$ perovskite films, when exposed to a humid environment for 15 days, show continuous degradation while the addition of 15% Cs to the film ($FA_{0.85}Cs_{0.15}PbI_3$) [88] and 20% Cs to the film ($FA_{0.8}Cs_{0.2}PbI_3$) [89] sustain high performance of the PV device without degradation [88]. Based on these assessments, the use of MA-free CsFA cation-based perovskites became a strategy for developing high-efficiency, stable cells. Rb-doped $CsFAPbI_3$ perovskites capable of a PCE > 20% have been reported as an example and can function for 1000 hours under continuous sunlight exposure [76]. In the industrial development of PSCs, the composition of $CsFAPb(I, Br)_3$ tends to be adopted by manufacturers of perovskite PV modules and tandem cells.

1.6 Strategies to Stabilize Halide Perovskite Solar Cells

1.6.1 Bridging the Gap Between Efficiency and Stability

The R&D efforts on halide PSCs have been enhancing the record value of PCE, which is now reaching the theoretical limit (SQ limit) in terms of the FF and output voltage [43, 44]. However, these PCE record values are not compatible with sufficiently high stability of the device in most cases. This differs from the case of commercialized high-performance devices using inorganic photovoltaic semiconductors, such as Si, GaAs, and CdTe, which can sustain high stability compatible with high efficiency. The instability of halide perovskite materials under high temperature and continuous irradiation is ascribed to the ionic mobility intrinsic to the ionic semiconductors [45], in which highly diffusible halide anions are largely responsible for this problem. Ionic diffusion is also assumed to cause anomalous hysteretic behavior of the photocurrent in *J–V* performance [90–92] (see Chapter 7), which can be enhanced in the presence of structural defects or voids at the interface of the perovskite and

charge transport layers [93–95]. Despite these drawbacks, the strong ionic character of the metal halide structure contributes to stabilizing free carriers via the charge screening effect assumed to result in an excellent PV performance of the halide perovskite. Therefore, stability and high performance often have a trade-off relationship. To overcome this dilemma, compositional engineering should be directed not only to reduce the ion diffusion inside the perovskite crystals but also to modify the chemical structure of heterojunction interfaces where mobile ions can diffuse beyond the interfaces to interact with the adjacent layers. Simultaneous improvement of efficiency and stability has also been achieved by improving the morphology and physical quality of solution-processed perovskite films. While the use of large grains and high crystallinity of perovskite leads to high efficiency, large grains and a dense uniform morphology are advantageous for improving the stability. Figure 1.11 shows an example of a high-efficiency (>21%) triple-cation PSC fabricated under ambient conditions in our lab [96]. This large-grain perovskite film maintains its high PCE for storage of the cell exposed to ambient air for more than five months.

The triple-cation recipe was then followed by a quadruple-cation mixed perovskite that included Rb as the fourth cation. With the mixed perovskite composition (5% of

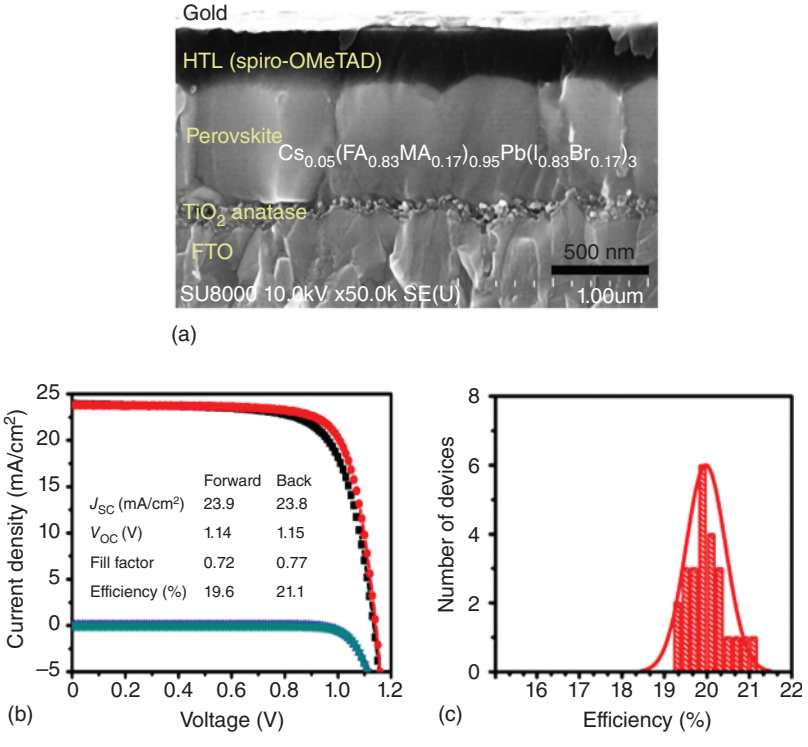

Figure 1.11 Cross-sectional SEM image (a), current density–voltage (J–V) curves (b), and PCE histogram plot (c) of triple-cation perovskite solar cells fabricated in ambient air under controlled humidity (15–25%). Source: Reproduced with permission from Miyasaka [10]. Copyright 2018, Chemical Society of Japan.

Rb, E_g of 1.63 eV), Saliba et al. achieved stabilized efficiencies of up to 21.6%, and the polymer-coated cells maintained 95% of their initial performance during 500 hours of operation at the maximum power point (MPP) at 85 °C [97]. In comparison with Cs/FA/MA triple-cation devices, Rb-based quadruple-cation perovskite cells show greater photostability, which can be attributed to reduced recombination and fewer defects [98].

1.6.2 Enhancing Intrinsic Stability of Halide Perovskites

The structural/intrinsic stability of perovskites has become the most important parameter for assessing the long-term durability of PSCs. For outdoor installations such as Si PV panels, PSCs must guarantee the production of stable power at operating conditions of real sunlight radiation, raised temperature due to heating, and atmospheric moisture and oxygen for a period of >20 years. Thus, these conditions are considered as the requisite for the commercialization of PSCs in outdoor PV panels. Long-term stability issues with perovskite include both intrinsic and extrinsic stability. Moreover, extrinsic stability is affected by environmental stresses such as heat, light, humidity, and oxygen. Both types of stabilities are critically important to suppressing the deterioration of PV devices under continuous operation. The intrinsic structural stability of perovskites can be primarily judged by the Goldschmidt tolerance factor (τ) of the crystal, where $\tau = \frac{r_A + r_X}{\sqrt{2}\,(r_B + r_X)}$ and r_A, r_B, and r_X indicate the ionic radii of A, B, and X. The value of τ varies with the size of the ions in ABX_3. Since the ionic radii of organic cations (A) cannot be determined accurately, a certain amount of uncertainty lies in the calculated tolerance factors. Figure 1.12 shows the calculated tolerance factors of $APbI_3$ systems where A = Na, K, NH_4, Rb, Cs, MA, FA, ethylamine (EA), and ethylenediamine (EDA). When τ is in the range of $0.8 < \tau < 1$, ideal cubic perovskite structures or distorted perovskite structures with tilted octahedra are favored. Specifically, $0.9 < \tau < 1$ favors a cubic perovskite structure, while for $0.8 < \tau < 0.9$, a distorted perovskite structure is formed. Values of $\tau < 0.8$ and $\tau > 1$ diminish the possibility of the perovskite structure formation. Therefore, it can be expected that τ close to the middle of the range from 0.8 to 1, away from both the non-perovskite zones, would form a stable perovskite [99]. For $FAPbI_3$, τ is close to 1, which is near the upper boundary of the perovskite structure; therefore, $FAPbI_3$ is prone to the formation of a hexagonal δ-phase, which is photoinactive. An all-inorganic composition, $CsPbI_3$, with $\tau \sim 0.8$ is at the edge of the lower boundary for perovskite structures and normally crystallizes into a δ-phase. $MAPbI_3$ with $\tau \sim 0.9$ is close to the middle of the perovskite zone and exhibits the stable formation of a photoactive perovskite phase (showing a black color), although it has low thermal stability due to the volatile MA group.

As discussed in Section 1.5, the compositional engineering of perovskite by mixing different cations and anions improves the structural stability of perovskites, essentially by adjusting the value of τ close to the middle of the perovskite zone. The addition of Cs or MA to $FAPbI_3$ moves the τ value down from 1 to stabilize the cubic phase of $FAPbI_3$. For mixed perovskites, a simple mixture rule can be applied

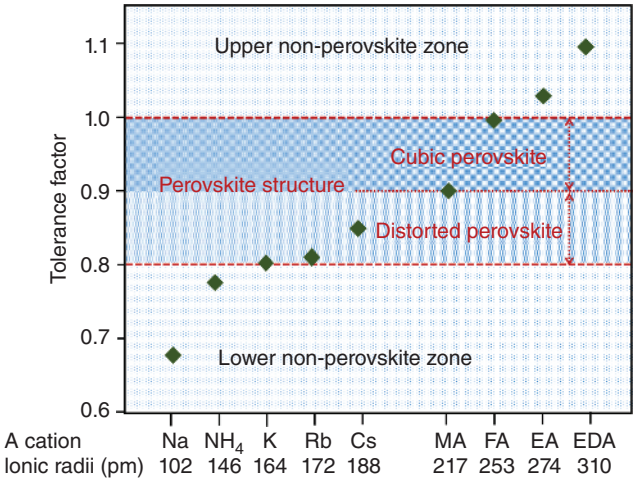

Figure 1.12 Calculated tolerance factors (τ) for different cations (A) in $APbI_3$ perovskite system. Commonly used cations like Cs, MA, and FA present τ in the range of 0.8–1.0, indicating the cubic perovskite phase structure. Ionic sizes of A cations used in calculation are values referring to 12-fold coordination (surrounded by 12 anions). Ethylammonium (EA) and ethylenediamine (EDA)) cations are too large, giving rise to τ values >1.0, and thus fall into the "upper forbidden zone" and cannot form perovskite alone. The group I alkali metal cations (Na, K, Rb) and NH_4 have a τ value <0.8 and fall into the "lower forbidden zone," not forming perovskite. However, all cations of lower or upper "forbidden zones" can be used as additives into those cations in "cubic perovskite formation zone" for phase stabilization.

to obtain an approximate value of the effective tolerance factor. According to the mixture rule, for a perovskite with composition $(A_xA'_{1-x})B(X_yX'_{1-y})_3$, effective cation radius and anion radius, namely, $r_A(\text{eff})$ and $r_X(\text{eff})$ can be calculated by the following equations:

$$r_A(\text{eff}) = x\,r_A + (1-x)\,r_{A'}, \text{ and } r_X(\text{eff}) = y\,r_X + (1-y)\,r_{X'} \tag{1.1}$$

The effective tolerance factor (τ_{eff}) of a mixed perovskite, $(MAPbBr_3)_{0.15}(FAPbI_3)_{0.85}$, calculated using the values of $r_A(\text{eff})$ for MA, FA, and $r_X(\text{eff})$ for halogen is ~0.98 while that for triple-cation mixed perovskite with 5% Cs (i.e. $Cs_{0.05}(MA_{0.17}FA_{0.83})_{0.95}Pb(I_{0.83}Br_{0.17})_3$) is ~0.97. From such values of τ_{eff}, it can be assumed that more Cs or MA in these mixed perovskite systems should result in even more stable perovskite structures. However, for such mixed perovskites, the formation of secondary non-perovskite phases above a certain concentration becomes another important factor that influences the stability; τ_{eff} close to 0.9 is therefore not a sufficient condition for predicting the structural stability of mixed perovskites. Nonetheless, it provides guidance for selecting ions or a combination of ions [99]. Cations with large differences in the ionic sizes between the additive (Na, K, Cs, Rb) and the matrix system (FA/MA mix) are preferred for stabilizing the perovskite structure as long as there is no non-perovskite secondary structure. In other words, phase purity also plays a significant role in the intrinsic long-term stability of the mixed perovskites. The crystal structure difference between $MAPbI_3$

(tetragonal) and mixed perovskites (FA-MA-Cs) (usually cubic) might also be the reason why mixed perovskites are more stable. As cubic structures with higher symmetry than tetragonal structures are more stable, mixed perovskites with cubic structures show better stability than pure $MAPbI_3$. Moreover, thermodynamic stability of different perovskite compositions will provide better insights into structural/intrinsic stability of different perovskites. At high temperatures, $MAPbX_3$ (X = Cl, Br, I) decomposes into PbX_2 (s), MA (g), and HX (g). The energy of formation of these decomposed components confirms that $MAPbI_3$ and $MAPbBr_3$ are thermodynamically more stable than $MAPbCl_3$ [100]. With regard to the actual long-term stability of mixed-cation perovskites, Saliba et al. demonstrated that $Cs_x(FA_{0.83}MA_{0.17})_{(1-x)}Pb(I_{0.83}Br_{0.17})_3$ is stable under continuous operation exposed to 1-sun illumination for 250 hours while the Cs-free $FA_{0.83}MA_{0.17}Pb(I_{0.83}Br_{0.17})_3$ structure degraded within 50 hours [66]. A similar $CsFAMAPbI_{3-x}Br_x$ cell achieved a lifetime of >1000 hours under 1-sun illumination using a CuSCN layer as an HTM [101]. A recent analysis of the multi-cation perovskite decomposition process has confirmed that Cs inclusion increases the thermal stability of $FA_{0.85}MA_{0.15}$ $Pb(I, Br)_3$ perovskite [102]. The structural stabilities of mixed-cation perovskites are summarized in review articles [103].

Ion migration in the halide perovskite crystal also triggers the degradation of materials. It can cause anomalous *J–V* hysteresis, phase segregation, and deterioration of the long-term stability of PSCs [45]. In any ionic solid, the migration of ions must be mediated by defects in the solid. It is believed that ions in perovskites essentially migrate through the cation and anion defects (i.e. MA^+ and I^- vacancies). The ease of migration of an ion in a perovskite film can be assessed by its activation energy of migration. Calculation of activation energies of migration for different constituting ions (i.e. I^-, Pb^{2+}, and MA^+ of FA^+) in perovskites suggests that iodide is the most easily migrating ion [104], which is consistent with experimental studies [105, 106]. MA^+ cations also migrate in perovskite crystals [107]. In polycrystalline films, the preferred regions of ion migration are considered to be grain boundaries rather than within the grains. Therefore, it is possible to minimize ion migration by reducing the number of grain boundaries or by increasing the grain size. However, the evidence of ion migration occurring within single crystals of $MAPbI_3$ [108] and $MAPbBr_3$ [109] indicates that suppression of ion migration requires a fundamental change in the perovskite composition.

1.6.3 External and Environmental Stability

In addition to the intrinsic stability of perovskites, the stability of perovskite-based devices is affected by external conditions such as moisture, oxygen (air), heat, light, and external bias, which can degrade the device structure involving the change of surrounding carrier transport materials. Because ionic conductors have some affinity for polar media, the sensitivity of perovskite to moisture (H_2O) has been a matter of concern for its long-term stability. It is known that water molecules easily bind to perovskite by hydrogen bonding to form hydrated compounds, which alter the properties of perovskite locally. The losses caused by this hydrated compound

can be reversed, as shown for $MAPbI_3$ in Eq. (1.2), but further ingression of water can cause irreversible degradation of perovskite to PbI_2 and other components (Eq. (1.3)) [110]:

$$4CH_3NH_3PbI_3 + 4H_2O \leftrightarrow 4\left[CH_3NH_3PbI_3{\cdot}H_2O\right] \leftrightarrow (CH_3NH_3)_4PbI_6 \cdot 2H_2O + 3PbI_2 + 2H_2O \quad (1.2)$$

$$(CH_3NH_3)_4PbI_6 \cdot 2H_2O \rightarrow 4CH_3NH_3I + PbI_2 + 2H_2O \quad (1.3)$$

Therefore, the proper encapsulation of PSCs with films of gas barrier functions is a prerequisite for the prevention of degradation caused by moisture. On the other hand, many efforts have been made to improve the moisture resistance of materials constituting the cell structure, either by introducing hydrophobic layers such as polymer/carbon composites in place of the widely used spiro-OMeTAD [111] or by incorporating non-hygroscopic interlayers between perovskite and HTMs [112, 113] or by passivating (modifying) the perovskite surface with small molecules [114]. For instance, tetra-ammonium zinc phthalocyanine has been employed to passivate the grain boundary of $MAPbI_3$ [115], and the stabilized device showed a long lifetime of 1000 hours, sustaining 90% of PCE for storage at 85 °C and 45% humidity.

A recent major trend in modifying the surface and grain boundaries of perovskite films is to incorporate a 2D perovskite material with a hydrophobic organic group into the general 3D perovskites [116]. The mixing a small amount of 2D materials is very promising in terms of reinforcing stability. This serves two purposes: passivation of the traps and protection against moisture ingression. Large organic cations in 2D perovskites are more hydrophobic than MA and FA and help to increase the moisture resistance [117, 118]. 2D perovskites have intrinsically low PV performance because of their narrow light absorption band in addition to poor electron-transport properties due to the mixing of insulating organic groups [119]. However, mixing a small amount of 2D perovskites to 3D perovskites can increase efficiency and improve long-term stability. Several 2D/3D mixed perovskite compositions and their cell efficiencies and stabilities are listed in Table 1.3. For instance, the incorporation of 0.8 mol% of ethylenediammonium iodide (EDAI) (which forms a 2D perovskite structure $EDAPbI_3$ when mixed with PbI_2) into a 3D $MAPbI_3$ structure improves the PCE by reducing recombination [121] and enables stable operation of the device at 50 °C and 50% relative humidity under illumination while the regular $MAPI_3$ loses 90% of its initial PCE in just 15 hours (Figure 1.13). Similarly, phenylethylamine iodide (PEAI), which was employed to deposit PEA_2PbI_4 capping layers on top of the 3D perovskite film, improved the long-term stability of the cell, retaining nearly 90% of the initial PCE after 1000 hours exposure in ambient conditions with a high relative humidity of 60% ± 10% [125]. The hydrophobic nature of the trifluoroethylamine (FEA) chain was applied to incorporate 2D perovskites, $(FEA)_2PbI_4$, in triple-cation 3D perovskite, $(FA_{0.825}MA_{0.15}Cs_{0.025})\ Pb(I_{0.85}Br_{0.15})_3$, to reinforce moisture resistance (Figure 1.14) [122]. A cell using FEA-modified perovskites without encapsulation maintained over 90% of the initial PCE (18%) under 65% humidity at room temperature for up to 28 days (Figure 1.14b). FEA-based perovskite was also introduced to

Table 1.3 List compositions of 2D/3D mixed perovskites, corresponding solar cell performance and stability.

Spacer cation	Mixed perovskite	Device structure	PCE (%)	Stability	References
Butylamine (BA)	$BA_{0.09}(FA_{0.83}Cs_{0.17})_{0.91}Pb(I_{0.6}Br_{0.4})_3$	FTO/SnO_2/C60/perovskite/spiro-OMeTAD	17.2	Retaining 80% of initial performance up to 1000 h (non-encapsulated cells), above 3000 h (encapsulated cells)	[120]
Ethylene diamine (EDA)	$MA_{1-2x}EDA_xPbI_3$ ($x = 0.008$)	FTO/c-TiO_2/perovskite/spiro-OMeTAD/Au	17.6	Retaining 75% of initial performance after 72 h under AM 1.5G irradiation, 50% relative humidity (RH), 50 °C device temperature	[121]
$CF_3CH_2NH_2$	$[CF_3CH_2NH_2]_2(FA_{0.825}MA_{0.15}Cs_{0.025})_{n-}Pb_n(I_{0.85}Br_{0.15})_{3n+1}$	FTO/c-TiO_2/m-TiO_2/perovskite/spiro-OMeTAD/Au	18	Better stability than 3D under 65% RH for up to 4 weeks	[122]
Butylamine (BA)	$(BA)_2(MA)_{n-1}Pb_nI_{3n+1}$	ITO/PTAA/perovskite/PCBM/C60/BCP/Cu	>18	Better thermal stability than 3D perovskite	[120]
Phenylethylamine (PEA)	$FA_xPEA_{1-x}PbI_3$	ITO/NiO_x perovskite/PCBM/C60/Ag	17.7	Stability measured at maximum power point up to 2 weeks, better stability than 3D structure	[123]
PEA	$Cs_{0.1}FA_{0.9}PbI_3$	FTO/TiO_2/perovskite/spiro-OMeTAD/Au	20.3	82% of its initial efficiency sustained after continuous 1-sun illumination at 40 °C for 800 h under N_2 atmosphere	[124]

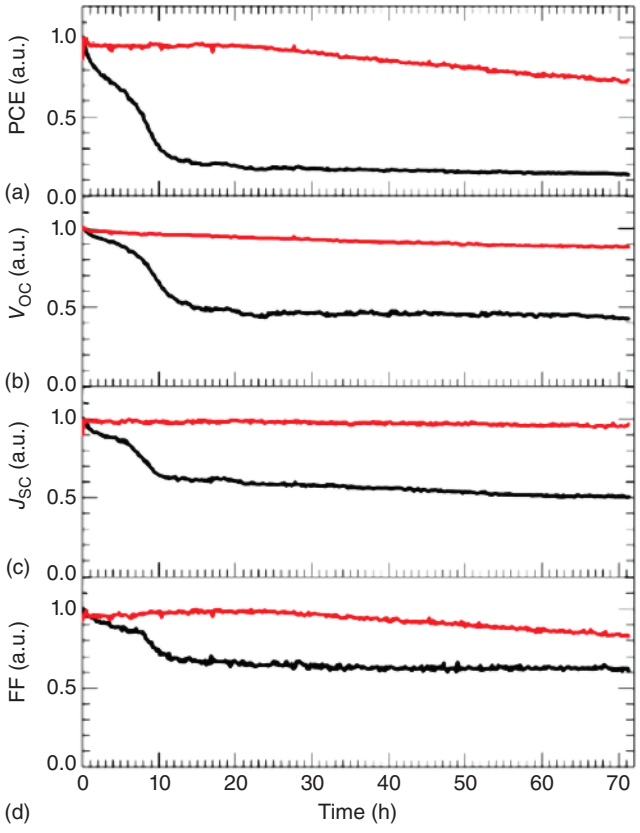

Figure 1.13 Long-term evolution of normalized (a) PCE, (b) V_{OC}, (c) J_{SC}, and (d) FF for the planar PSCs based on pristine $MAPbI_3$ and $MA_{1-2x}EDA_xPbI_3$ ($x = 0.008$) tested under 1-sun illumination at 50 °C and 50% relative humidity. Source: Lu et al. [121].

protect the interface of perovskite and stabilize the cell under 50% ± 5% humidity for 60 days [126]. As alkyl diammonium, butanediamine iodide ($BEAI_2$) forms a 2D perovskite interlayer to passivate the grain boundaries of perovskites and stabilizes high-performance cells (PCE > 19%) at a high temperature (85 °C) in ambient air and under continuous illumination [127]. 5-Aminovaleric acid iodide (AVAI) has become a popular material for stabilizing $MAPbI_3$ since it has been employed in dopant-free carbon-based PSCs [128]. Three mole percent of AVAI added to $MAPbI_3$ perovskite stabilizes a carbon-based PSC device, and a large module ($10 \times 10\ cm^2$) of the device exhibited stability for more than 10 000 hours (>1 year) at 55 °C under 1-sun illumination [129]. It has been reported that when a cesium salt of 5-aminovaleric acetate replaces 5-aminovaleric acid in a carbon-based structure, the intrinsic thermal stability of $MAPbI_3$ is improved to have a 500-hour lifetime at 100 °C in a glove box [130]. Carbon-based PSCs have relatively high thermal stability owing to the use of dopant-free chemically stable carbon layers. The recent progress of carbonaceous material-based PSCs is summarized in a review [131].

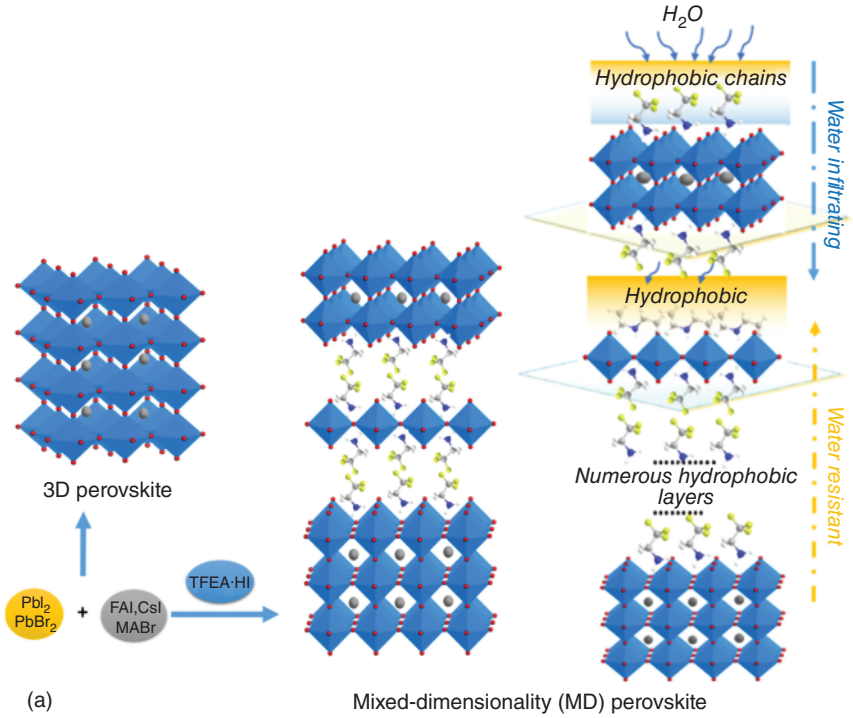

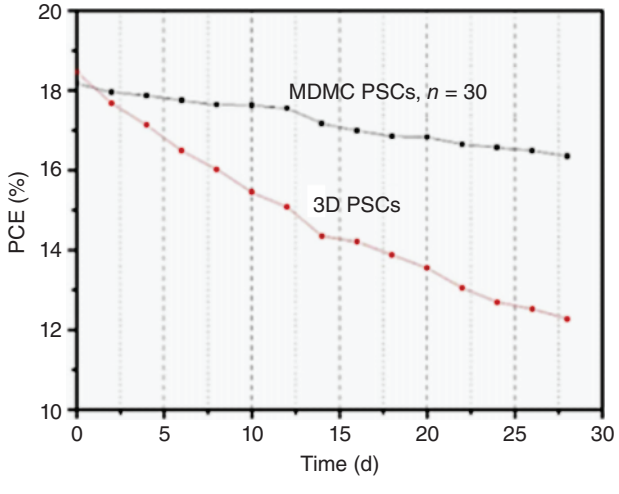

Figure 1.14 (a) Schematic representation of the stacking structures of multidimensional multicomposition (MDMC) perovskites based on trifluoroethylamine ammonium cations, (b) power conversion efficiency (PCE) as a function of storage (under a relative humidity level of 65% at room conditions) time for conventional 3D and MDMC (n = 30) perovskite solar cells, tested using an interval of one day. Source: Ye et al. [122].

The moisture resistance of PSCs can also be enhanced by modifying the perovskite surface with hydrophobic polymers. For instance, an ultrathin layer (<10 nm) of polyvinylpyridine (PVP) coated on the perovskite surface ($MAPbI_3$) and in contact with spiro-OMeTAD improves the water resistance of $MAPbI_3$ when dipped in water for up to 100 seconds. PVP-modified device also shows enhanced open-circuit voltage and efficiency [112]. The Lewis base side chain of PVP possibly coordinates the undercoordinated Pb^{2+} on the surface of the perovskite, thereby reducing the surface trap density as observed by PL enhancement. A similar result was also reported by Tress and coworkers who found a large effect of suppressing non-radiative recombination using PVP as a thin interlayer and succeeded in elevating V_{OC} to 1.20 V [132]. Furthermore, the continuous chemical functionalization of the grain boundaries of $MAPbI_3$ films using triblock copolymers that exhibit both hydrophilicity and hydrophobicity has also been found to boost the PCE (>19%) and the stability of $MAPbI_3$ cells [133].

Although surface modification using 2D perovskites and hydrophobic polymers is effective in raising the moisture (H_2O) resistance, the perovskite film also shows a high sensitivity to atmosphere (O_2, N_2, or vacuum), the influence of which might become a greater concern than humidity in terms of the necessity to protect the device with gas barrier films. It has been found that perovskite films show weak PL in a vacuum or in N_2 and strong luminescence when aged in O_2. For instance, $MAPbBr_3$ single crystal exhibits PL intensities two orders of magnitude higher in air than in a vacuum [134]. As evident from another study, O_2 is reversibly adsorbed on the surface of $MAPbI_3$ (Cl) and passivates the deep surface trap states, resulting in enhanced luminescence [135]. By investigating the simultaneous effect of light, moisture, and oxygen on perovskite ($MAPbI_3$), Stranks and coworkers found the involvement of superoxide ion ($O_2^{\cdot -}$) in defect passivation. According to them, O_2^- ions, formed in the presence of light, remove the shallow trap states at the surface of $MAPbI_3$, thereby enhancing the internal luminescence quantum efficiency (from 1% to 89%) [136]. Although oxygen can have a positive effect on defect passivation, Kong et al. showed a contradictory result based on Raman spectroscopy regarding the role of O_2 in oxidizing perovskite surfaces and deactivating luminescence [137]. Such oxygen-induced changes or degradation of perovskite can occur in a dry atmosphere (no moisture). Several studies have disclosed that perovskite films exposed simultaneously to oxygen and light degrade faster than even the moisture-exposure case. The suggested mechanism follows the generation of superoxide ($O_2^{\cdot -}$) by electron transfer from the photoexcited $MAPbI_3$ to oxygen and the decomposition of $MAPbI_3$ by deprotonation with $O_2^{\cdot -}$ to $CH_3NH_3 + PbI_2 + 1/2I_2 + O_2$ [138]. Thus, the incorporation of less acidic organic cations such as FA or inorganic cation Cs shows increased the durability of the films. In addition, the oxygen tolerance of perovskites strongly depends on charge carrier density; cells aged under open-circuit conditions (no charge collection) show faster degradation than the cells at short-circuit conditions [139]. Hence, the integration of an efficient electron-collecting layer (TiO_2, etc.) in the structure improves the stability by reducing the yield of superoxide ions [140].

Instability against moisture and O_2 can be partially or completely solved by external protection, but the effect of light (photo-instability) on perovskite is becoming a formidable issue. Almost all chemical processes such as ion migration, defect generation, and phase segregation, which affect the long-term stability of perovskites, are unfortunately found to be influenced by light, which must inevitably shine on the cells for their operation. Photocatalytic degradation by TiO_2 [141, 142], photoinduced ion migration [109], photoinduced trap-state generation [143], photoinduced phase segregation [144], photoinduced cation or halide redistribution [145], etc. have been found to be the reasons behind device performance deterioration under constant illumination. UV light-induced photocatalytic degradation by the most widely used ETM, TiO_2, can be prevented by the replacement of TiO_2 with an alternative, less photoactive electron transport layer (ETL) such as Al_2O_3 [141] or SnO_2 [146]. Even ETL-free devices using bathocuproine (BCP) as an interlayer between FTO and perovskite have been observed to demonstrate superior stability under illumination than TiO_2-based devices [147]. In addition, coating a UV absorber such as an organic film (UV 234) on the front side of the substrate has also been effective in improving the UV irradiation resistance of the device [148]. However, photoinduced phase segregation or ion redistribution in mixed-halide (I and Br) perovskites is a serious issue to be solved. A reversible photoinduced phase separation results in the formation of iodide-rich and bromide-rich regions [149] in mixed-halide perovskites. Such I-rich and Br-rich phase separation leads to the generation of low-bandgap trap states, which causes performance degradation of the solar cells under illumination. While one of the proposed origin mechanisms for such phase segregation involves electron–phonon coupling in the photoexcited state of mixed perovskites deforming the surrounding lattice [144], the other proposed origin is halogen defects [150]. Based on the observation of less severe phase segregation in mixed-halide perovskites containing Cs or FA as partial substitution of MA, which eventually improves the crystallinity and morphology through large grains, it is believed that defects such as halogen vacancies are essentially the main promoters of such phase separation. As ion mobility in these materials is known to be more facile at the grain boundaries [151], reducing the volume of grain boundaries (growing large grains) by compositional tuning with Cs or FA results in improved photostability by slowing down ion migration. Phase segregation can be ignored when pure mono-cation/anion compositions such as $MAPbI_3$, $FAPbI_3$, $CsPbI_3$, etc. are used. In this regard, the use of $MAPbI_3$, which is relatively stable at room temperature and against humidity, is still promising if the device is perfectly protected by encapsulation. The stabilization of MA-containing mixed perovskites for practical use has been demonstrated recently with the detailed analysis of outgas on decomposition processes for the device encapsulated by gas barrier films. A polyisobutylene-based or polyolefin-based polymer–glass combination for encapsulation enables excellent durability exceeding the requirements of the IEC61215:2016 damp heat and humidity freeze tests [102]. Such state-of-the-art encapsulation methods are expected to stabilize $MAPbI_3$ devices against heat and light.

Finally, carrier-transporting materials that contact the perovskite layer also play a substantial role in changing the device stability. In addition to ensuring beneficial

activity in conducting carriers, they should be inert in chemical reactions with perovskites and stable against external impacts such as heat and humidity. HTM can be very critical for long-term stability because perovskite/HTM junctions are the "beating heart" of the whole device. Spiro-OMeTAD is an excellent HTM in terms of appropriate HOMO levels and is useful as a relatively thick film prepared by simple coating. However, spiro-OMeTAD requires mixing of ionic dopant (lithium bis(trifluoromethanesulfonyl)imide, Li^+TFSI^-, etc.), which promotes the oxidation of this HTM under ambient air to ensure normal hole conductivity. Such dopants, owing to their hygroscopic nature, allow the easy ingress of moisture into the film, which eventually degrades the perovskite film (turning yellow). Furthermore, ionic dopants diffuse to the perovskite layer across the junction interface and trigger deterioration of the device performance. Such diffusion can be accelerated at high temperatures or under ambient humidity. It is known that the spiro-OMeTAD layer undergoes deformation by generating many voids inside the layer upon heating to 100 °C [152, 153]. The mechanism of device degradation includes not only the dopant diffusion of HTM but also ionic migration from perovskites. For example, spiro-$OMeTAD^+$ can react with migrating I^- to lose its hole conductivity [154], and MA^+ ions migrated from $MAPbI_3$ react with spiro-OMeTAD to cause performance degradation [155]. Therefore, the prevention of ion diffusion between the layers is one of the strategies to improve the thermal stability of PSCs. To prevent iodine diffusion from perovskite ($FA_{0.85}MA_{0.15}Pb(I_{0.85}Br_{0.15})_3$) to spiro-OMeTAD, an ultrathin layer of Al_2O_3 (~1 nm) coated by atomic layer deposition on the perovskite layer was found to effectively block ion diffusion across the interface [156]. For such a thin Al_2O_3 layer, its insulating property to reduce the photocurrent is generally negligible. Apart from instability, another problem with spiro-OMeTAD is the high cost of the material. To replace spiro-OMeTAD, a great deal of effort has been expended to synthesize various types of organic HTMs for use in PSCs [157]. These HTMs are either small molecules or hole-conducting (p-type) polymers. Conducting polymers are represented by P3HT, PTAA, PEDOT:PSS, etc. Poly-triarylamine (PTAA) has been employed to record the highest efficiency of PSCs [158]. However, organic HTMs, including these polymers, are intrinsically low in conductivity and require the use of p-dopants and/or additives, similar to spiro-OMeTAD. Therefore, their dopants still retain the risk of decreasing the device stability.

A solution to avoid the degradation caused by organic HTMs is to develop a dopant-free HTM bearing no ionic moieties in its structure. Inorganic HTMs as p-type conductors can meet this purpose. They are oxide or compound semiconductors such as NiO_x [159, 160], CuO_x [161, 162], Cu_2O [163], CuI [164, 165], Cu(thiourea)I [166], CuSCN [101, 167], $CuGaO_2$ [168], $CuCrO_2$ [169], and Cu phthalocyanine [170]. Promisingly, many of them have achieved comparable efficiency and longer life than spiro-OMeTAD. Aside from the use of these inorganic hole conductors, the development of dopant-free organic HTMs is becoming a main strategy to stabilize PSCs. Although organic HTMs are thermally less stable than inorganic HTMs, they can have higher chemical and electrochemical stabilities than inorganic materials against oxidation and attack of the halide anions of perovskites. Many dopant-free organic HTMs in small molecules or polymeric

materials have been shown to achieve PCEs in excess of 18%. [171]. As a small molecule, a truxene core-introduced OMeTAD derivative achieves a high PCE of 18.6% without the addition of dopants [172]. A conjugated small-molecule HTM containing a benzothieno-pyrrole core enabled an efficient PSC device (PCE > 18%) to have a long lifetime for 33 days of storage [173]. Cao et al. employed a spiro-based dopant-free HTM containing redox-active triphenyl amine units that undergo molecular organization normal to the substrate. A device with this organized HTM layer yielded a PCE of 20.6% [174]. Donor–π–acceptor-type (D–π–A) molecules have been developed for new HTMs in which intramolecular charge transfer in the D–π–A molecule is assumed to eliminate the need for dopants or additives in the HTM. A device using an HTM molecule consisting of a quinolizino acridine donor and terthiophenes and malononitriles as acceptors functions with a PCE of 18.9% with superior long-term stability under 1300 hours of illumination [175]. A compound having a triphenylamine donor and a thienopyrazine unit as the acceptor was presented as a D–A–D-type HTM, which yielded a PCE of 19.27% with a high V_{OC} of 1.11 V [176]. Phthalocyanine (Pc) derivatives are known as thermally robust organic pigments and p-type semiconductors. They also work well as dopant-free HTMs with excellent moisture resistance and high thermal stability [177]. For example, a thin film of a butyl derivative of copper Pc (CuPc) coated on a high-efficiency perovskite absorber ($Cs_{0.07}Rb_{0.03}FA_{0.765}MA_{0.135}PbI_{2.55}Br_{0.45}$) achieved PCE values exceeding 20%. The same CuPc film coated on a more thermally stable MA-free CsFA perovskite absorber exhibited high thermal stability for the device after >2000 hours of storage at 85 °C in an N_2 atmosphere and light soaking stability for 100 hours [178]. Besides these small molecule HTMs, polymer HTMs is also sought due to their hydrophobic nature ensuring moisture resistance in addition to good thermal stability. Unlike PTAA-type polymers, which work at high efficiency with dopants, dopant-free polymer HTMs are mostly based on thiophene backbone chains, similar to the structure of P3HT [171]. For efficient electronic devices, HTM is required to exhibit a hole mobility of more than 10^{-4} $cm^2/(V\,s)$. The polythiophene family is capable of this mobility level without dopants, which is higher than the mobility of PTAA (10^{-5} $cm^2/(V\,s)$). For example, a dopant-free copolymer comprising ethylhexyloxy phenylene and bithiophene units, which was employed in a PSC device with an inverted structure, showed a PCE of 19.5% (certified) [179]. D–A-type thiophene-based copolymers are also capable of high hole mobility without the use of dopants. D–A-type copolymers (asy-PBTBDT) comprising benzodithiophene and benzothiadiazole (BT) as donor and acceptor units, respectively, had their contact with the perovskite layer improved with the introduction of tetraethylene glycol chains on BT units. The dopant-free devices yielded PCEs of up to 19.8% with a high V_{OC} of 1.14 V [180]. Reflecting on the effect of polymer HTMs as protective layers, most of these polymer HTM-based PSCs have a shelf life of more than 30 days under ambient air. A new dopant-free copolymer was recently developed in our group. Comprising 2,5-pyrroledione and bithiophene units, an alternating copolymer, poly(DTSTPD-*r*-BThTPD), has a high hole mobility of 1.5×10^{-3} $cm^2/(V\,s)$ and is thermally stable up to 330 °C [181]. Although its HOMO level of −5.44 eV is much lower than that of P3HT (−4.94 eV)

or PTAA (−5.14 eV), this dopant-free polymer exhibited high PV performance for all-inorganic perovskite cells using $CsPbI_2Br$ as an absorber, whose HOMO level is located at approximately −5.58 eV, slightly lower than that of the HTM (Figure 1.15). As described in the next section 1.7, this dopant-free $CsPbI_2Br$ solar cell, which absorbs wavelengths up to 650 nm (bandgap of 1.92 eV), yielded a PCE of 15.5% and a significantly high V_{OC} value of 1.43 V when TiO_2 ETL was replaced with an amorphous SnO_2 ETL [69]. In summary, a strategy to develop methods for stabilizing perovskite devices by blocking the ion diffusion across the junction interfaces is to combine these dopant-free and high-efficiency HTMs with 2D-based stabilized compositions of perovskites. This direction is expected to enable the development of high-performance, robust PSCs for practical device implementations.

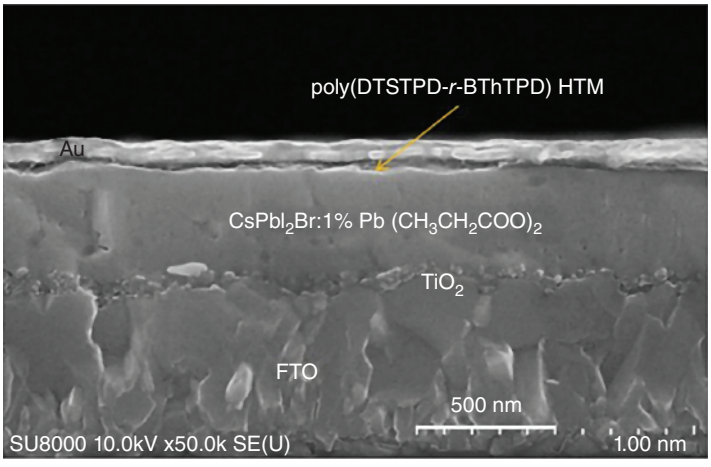

(a)

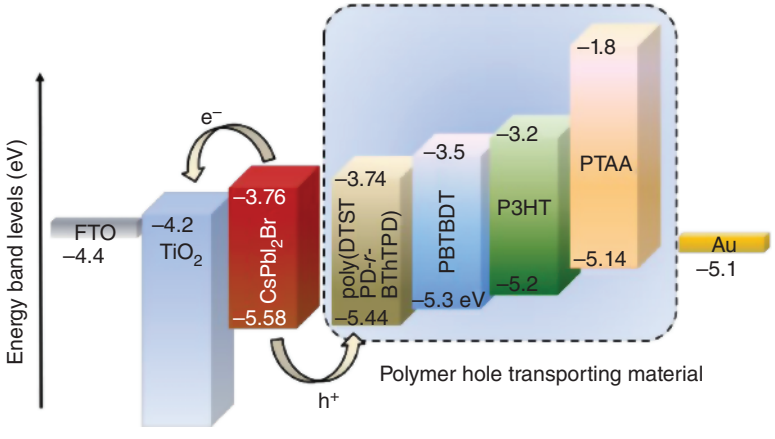

(b)

Figure 1.15 Polymer hole transport materials (HTMs). A thin film (20–40 nm) of HTM (poly(DTSTPD-r-BThTPD)) coated on the perovskite $CsPbI_2Br$ layer (a) and the relation of polymer HTM energy levels with respect to $CsPbI_2Br$ (b). Source: Reproduced with permission from Öz et al. [181]. Copyright 2020, American Chemical Society.

1.7 Progress of All inorganic and Lead-Free Perovskites

Although the stabilities of organic–inorganic hybrid perovskites can be improved by interfacial engineering using 2D materials, the intrinsic thermal stability of perovskites is limited as long as they contain organic moieties such as the volatile MA. In this regard, the design of organic-free (all-inorganic) compositions for photovoltaic (PV) absorbers can be a way to guarantee the thermal robustness of the device. Cs-based lead perovskites with good thermal stability have been extensively studied for this reason. However, $CsPbI_3$ undergoes chemical equilibrium changes depending on the temperature. For example, the photovoltaically active black phase of α-$CsPbI_3$ (cubic) can be stabilized at temperatures above 310 °C [182], while the inactive yellow phase δ-$CsPbI_3$ (orthorhombic) tends to dominate the crystal at room temperature. Furthermore, $CsPbI_3$ absorbs moisture due to its hydrophilic nature. Despite this difficulty, PCE of $CsPbI_3$ PSCs has increased from 2.9% in the very first experiment by Snaith and coworkers [182] in 2015 to 18.4% in a recent work undertaken by Wang et al. [183], who found that the β-phase (tetragonal) of $CsPbI_3$, which is a photoactive black phase (E_g, 1.68 eV), can be stabilized at room temperature and its PV performance is enhanced by an additive that tunes energy levels of the β-phase and increases the interfacial contact between $CsPbI_3$ and ETL (TiO_2). There are other ways to stabilize the black active phase by introducing 2D perovskite such as ethylene diamine lead iodide ($EDAPbI_4$) [184]. We found that the inclusion of $Eu^{2+/3+}$ into $CsPbI_3$ can stabilize the black α-$CsPbI_3$ phase at room temperature by improving the quality of the polycrystalline film [185]. Another study succeeded in the formation of a stable black phase by improving the quality of α-$CsPbI_3$ and achieving a PCE of 15.7% [186]. An additional research direction for Cs-based inorganic perovskites is to enhance the PV functions of Br-mixed $CsPbI_3$, which have wider bandgaps depending on the fraction of Br/I. Br substitution in $CsPbI_3$ lowers the black phase formation temperature from 350 °C to approximately 250 °C and improves stability against phase transition. Although pure $CsPbBr_3$ having a wide bandgap of ~2.3 eV is not suitable as a sunlight absorber, bromoiodide perovskites $CsPbI_3Br_{3-x}$ with narrower bandgaps show promise for application in the top cell of tandem solar cells or indoor PV cells. In particular, indoor PV devices, used as a power source for internet of things (IoT) goods and equipment, work at high efficiency in harvesting LED illumination (wavelengths, <700 nm) using an absorber (semiconductor) that has a spectral sensitivity only to visible light ($E_g > 1.8$ eV). The bandgap of $CsPbI_{3-x}Br_x$ can be precisely controlled by the I/Br ratio. $CsPbI_2Br$, with an E_g of 1.9 eV, is an optimal composition for harvesting visible light and is highly stable at room temperature. When used in PV cells of inverted configuration using NiO_x as the HTM layer (HTL) and fullerene as the ETM layer (ETL), Liu et al. [187] obtained a PCE of 13.3% in the best cells. The cells showed superior long-term stability by exposing the non-encapsulated devices at 85 °C under N_2 atmosphere for 360 hours while a reference hybrid cell using $(CsFAMA)PbI_{0.85}Br_{0.15}$ lost 50% of their initial PCE after ~190 hours. Using $CsPbI_2Br$, our group obtained a PCE of 15.5% by enhancing the device V_{OC} up to 1.43 V [69], which is the highest V_{OC} so far obtained with visible light-harvesting

PSCs. The device was fabricated using an SnO_2 ETM in which the surface in contact with the $CsPbI_2Br$ layer was modified with a thin amorphous SnO_x layer (< 10 nm) to block hole injection and reduce the interfacial charge recombination. The HTM was a dopant-free polymer DTSTPD-*r*-BThTPD, as described in Figure 1.15. The high V_{OC} obtained with this cell configuration approaches the SQ limit of V_{OC} (see Section 1.4), leaving a voltage loss less than 0.5 eV. Figure 1.16 shows the scanning electron microscope (SEM) image of the device structure and *J*–*V* characteristics, which have a small hysteresis between forward and backward scans. The device, composed of a fairly thick and flat $CsPbI_2Br$ active layer and very thin HTL and ETL, can be characterized as a planar cell. The PCE of this dopant-free $CsPbI_2Br$ device was increased to 17.4% by replacing the above THM with a new donor-acceptor type conjugated copolymer HTM. Thanks to high V_{OC} characteristics, the device was found to work as an efficient indoor IoT PV device keeping a V_{OC} over 1.1V even under weak LED illumination (200 lx luminance) and exhibit a high PCE of 34% [189].

In the design of all-inorganic perovskites, an important direction toward their commercialization is the preparation of metal halide compounds that do not contain environmentally harmful lead, one of the ten most toxic elements for human health, as reported by the World Health Organization (WHO). Its toxicity has the potential to cause irreversible health effects affecting the central nervous, hematopoietic, hepatic, and renal systems, producing serious disorders [188]. As lead-free metal halide materials, organic tin halide perovskites such as $MASnI_3$, $MASnI_{3-x}Br_x$, and $FASnI_{3-x}Br_x$ have demonstrated the highest efficiencies in the field of lead-free perovskite photovoltaics [190]. The PCE of Sn-based perovskites has now reached 10% by compositional engineering using organic cations. However, Sn-based halide perovskites can function as efficient PV semiconductors as long as the reduced divalent form of Sn(II) is stabilized in an oxygen-free atmosphere. To overcome this issue, Diau and coworkers showed that a guanidinium (GA^+) cation-doped $FASnI_3$ crystal was stabilized in the presence of 1% ethylenediammonium diiodide ($EDAI_2$) as a 2D-forming additive, and the $GA_{0.2}FA_{0.8}SnI_3$-based device reached a PCE of 9.6% [191]. $EDAI_2$ was also applied to passivate $Cs_{0.2}FA_{0.8}SnI_3$ doped with SnF_2, and the device using this achieved a higher PCE (certified) of 10.08% [192]. Along with increasing efficiency, efforts to enhance the oxidation stability of Sn(II) have been made by incorporating reducing agents into the device structure [193]. Hayase and coworkers studied Sn-based perovskites to demonstrate a method to enhance efficiency and stabilize Sn(II) by compositional engineering. Diaminoethnae (DAE) was employed to passivate the defects of EDAI-doped $FASnI_3$ perovskites and DAE-based recombination suppression led to the highest PCE value of 10.18% [194]. More details on the progress of Sn-based hybrid perovskites are described in Chapter 10.

Sn-based and all-inorganic perovskites have also been studied for PV applications. They are Cs-based compositions, such as $CsSnI_3$ ($E_g \sim 1.3$ eV), $CsSnBr_3$ ($E_g \sim 1.8$ eV), $Cs_2SnI_4Br_2$, and $CsGe_{0.5}Sn_{0.5}I_3$ ($E_g \sim 1.5$ eV). However, their device performance is much lower than that of organic hybrid Sn perovskites [190] along with the stability issue of Sn(II). As a Sn(IV)-based composition, Cs_2SnX_6 (X = I, Br) is a fairly

stable Sn-based perovskite because Sn^{4+} does not oxidize, but this crystal exhibits poor mobility due to a structure consisting of isolated octahedron and may not be suitable for PV applications.

Lead-free all-inorganic perovskites have been studied intensively, focusing on group 15 metals such as Sb and Bi. In particular, as environmentally benign alternatives to Pb and Sn, Sb and Bi possess similar electronic configurations and comparable ionic radii with Pb, allowing them to incorporate effectively into the perovskite lattice. The crystal structure and optical properties of various ternary bismuth halide perovskite materials have been theoretically and experimentally investigated [195–197]. Although they have high stabilities against heat and moisture, PV devices using Bi perovskites have lagged behind lead-based or Sn-based

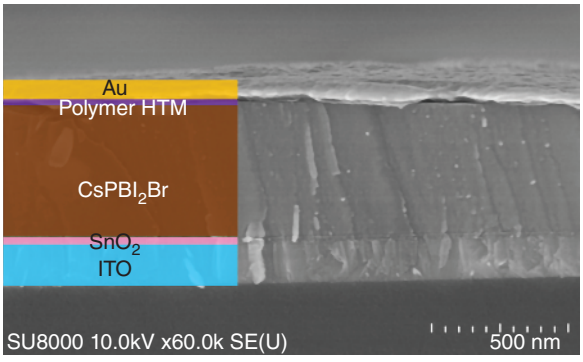

(a)

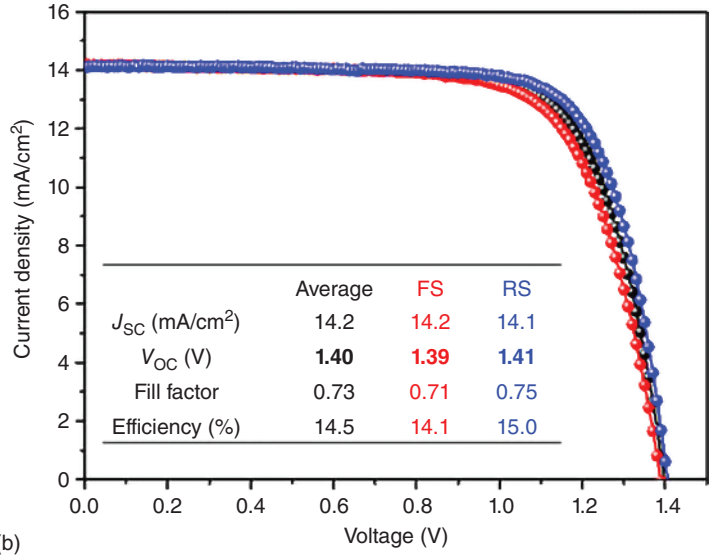

(b)

Figure 1.16 Layered structure of a $CsPbI_2Br$-based dopant-free HTM photovoltaic cell comprising ITO/SnO_2–SnO_x/$CsPbI_2Br$/poly(DTSTPD-*r*-BThTPD)/Au and its *J*–*V* characteristics showing a high V_{OC} of over 1.4 V. Source: Reproduced with permission from Guo et al. [69]. Copyright 2020, American Chemical Society.

perovskite PV devices in terms of efficiency development because of the large energy loss by carrier recombination, reducing J_{SC} and V_{OC}. This efficiency loss is primarily related to the poor morphology of the solution-processed polycrystalline film. We found that pinhole-rich morphology of $MA_3Bi_2I_9$ results from the fast crystallization of $MA_3Bi_2I_9$, and that retarding the crystallization by adding less volatile solvent (*N*-methyl-2-pyrrolidone) in the precursor improves the compactness of the film and enhances the $MA_3Bi_2I_9$ device performance [198]. However, the quality of Bi-based perovskite films tends to be inferior to those of Pb-based perovskite films, indicating difficulty in controlling the crystallization process based on chemical equilibria. To overcome this, Zhang et al. developed a non-equilibrium vacuum deposition process for obtaining good-quality $MA_3Bi_2I_9$ films in which a BiI_3 layer coated by vacuum deposition was transformed to $MA_3Bi_2I_9$ by reaction with MA under low vacuum. The method showed the formation of a pinhole-free, large-grain uniform layer with a charge-diffusion length and a density of trap states comparable with lead perovskite films [199]. Jain et al. developed a vapor-assisted solution process in which methylammonium iodide (MAI) vapor was exposed to the solution-processed BiI_3 film [200], enhancing the PCE of the $MA_3Bi_2I_9$ device up to 3.17% with $V_{OC} = 1.01$ V. All-inorganic analogs of Bi halide perovskites are more important for their robust stability. Silver bismuth halide, for example, $AgBi_2I_7$, is one of the potential candidates for all-inorganic lead-free PSCs. Sargent et al. prepared an $AgBi_2I_7$ (non-perovskite cubic phase) thin film from BiI_3 and AgI, and the PV cell created with this film exhibited 1.2% PCE and improved long-term stability against humidity and light soaking [201]. However, it is difficult to obtain high-purity single-crystal structures owing to the mixing of different phases (i.e. $AgBi_2I_7$, $AgBiI_4$, $AgBi_2I_5$, or Ag_3BiI_6) formed by the high-temperature annealing process. Addressing this phase impurity problem, we improved the solvent engineering process for obtaining phase-pure $AgBi_2I_7$. As a result, the PCE reached 2.1% [202]. However, there is a large PCE gap between Bi-based and Pb-based PSCs using all-inorganic perovskite compositions. The reason for this is that the use of ionic dopants (LiTFSI) to HTMs causes the chemical degradation of Ag/Bi perovskites. Therefore, the use of dopant-free HTMs becomes mandatory. Using P3HT as a dopant-free HTM, the device *J*–*V* performance of the Bi perovskites (Figure 1.17) shows that the efficiency of photocurrent generation is fundamentally low, yielding an external quantum efficiency (EQE) in a range of 20–40%. V_{OC} of 0.62 V shows a large loss from the bandgap of the material (1.78 eV). Such behavior of *J*–*V* characteristics indicates the existence of a large charge recombination in quantum conversion, which arises from direct recombination between CB and VB and from Shockley–Read–Hall (SRH) recombination associated with traps formed within the bandgap, leading to lower J_{SC} and V_{OC}, respectively [203]. The decrease in V_{OC} is mainly related to an increase in trap density, which has a high value in the grain boundary area rich in defects. Therefore, it is essential to enhance the device performance to improve the quality of the Bi perovskite film by forming a uniform pinhole-free morphology consisting of large grains. This strategy is common for all types of films consisting of lead-free inorganic perovskites, which tend to have low quality in terms of uniformity, compactness, and phase purity of crystals.

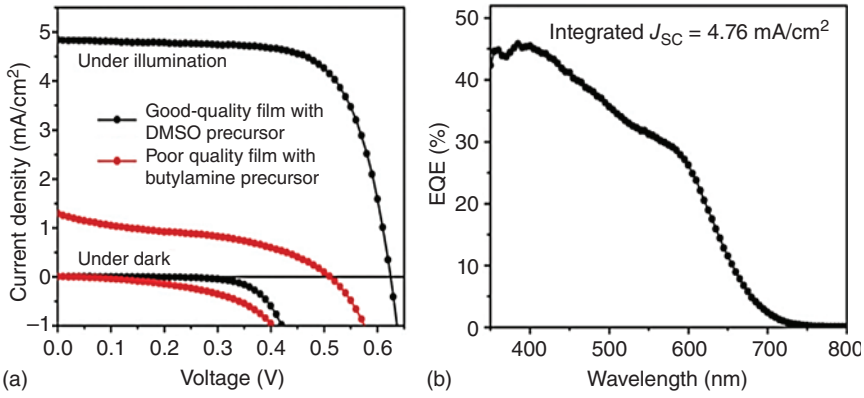

Figure 1.17 *J–V* characteristics (a) and EQE action spectrum (b) for $AgBi_2I_7$-based perovskite solar cells with dopant-free P3HT as HTM. In *J–V* curves, a good-quality perovskite film prepared from a dimethyl sulfoxide (DMSO) solution of precursor is compared with a film prepared from a butylamine solution. Source: Kulkarni et al. [202].

Antimony (Sb)-based halide perovskites also exhibit photovoltaic responses with their best efficiencies barely approaching those of Bi-based perovskites. $Cs_3Sb_2I_9$ has a high absorption coefficient with a direct bandgap of 2.05 eV. Prepared by the solution process, however, the $Cs_3Sb_2I_9$ films do not consist of a single phase of the 3D crystal but form a layered 2D phase and the 0D dimer phase of $Cs_3Sb_2I_9$. When Cs is replaced by Rb, $Rb_3Sb_2I_9$ is stabilized in the 2D layered form [204]. The device employing this $Rb_3Sb_2I_9$ perovskite shows a PCE of 0.66% while using $Cs_3Sb_2I_9$ results in a PCE of 0.84%. Much higher PCEs can be obtained with organic Sb perovskites such as $MASb_2I_9$. For example, the morphology of Sb perovskite films is improved by mixed-cation compositions, $A_3Sb_2I_9$ (A = Cs, MA), and the improved film quality leads to an increase in PCE up to 2.04% [205]. Furthermore, the incorporation of Cl^- into $MASb_2I_9$ was found to transform the dimer phase into a 2D phase, exhibiting PCE over 2% and stability of the device in dry air for 18 days [206]. Seok and coworkers synthesized a chalcogenide–halide mixed perovskite ($MASbSI_2$) [207], demonstrating the best PCE of 3.08% with optical gaps of 1.3–1.4 eV. The non-encapsulated $MASbSI_2$ device retained 90% of its initial efficiency when stored at ambient relative humidity of ~60%. Other interesting lead-free compositions are Ti(IV)-based halide perovskites such as Cs_2TiBr_6 with bandgaps of ~1.38 eV [208]. As a double perovskite, Cs_2TiBr_6 has achieved a PCE of above 3% with a simple device structure (FTO/TiO_2/Cs_2TiBr_6/P3HT/Au). However, the synthesis of pure Cs_2TiBr_6 requires highly controlled chemical and physical processes. Au-based perovskites such as $Cs_2Au_2I_6$ [209] have also been proposed as promising absorbers for photovoltaics. Although Au-based perovskites show theoretically good band structures and high optical properties, attempts to fabricate devices have not been successful, possibly because of the relatively high conductivities of the Au-containing material that can prevent good rectification of photocurrent generation. Many other candidates of non-lead perovskites for PV cells have been summarized in a recent review [210], in addition to Chapter 9 of this book

introducing the progress of new all-inorganic and all-inorganic lead-free perovskite materials.

1.8 Enhancing Efficiency of Low-Cost Tandem Solar Cells

Wavelength (bandgap) tunability of PSCs can facilitate the design of tandem cells, which is a combination of more than two cells with different spectral sensitivities (bandgaps) to enhance sunlight collection and gain a PCE that exceeds the maximum obtained by the highest-performing single cells such as crystalline silicon (Si) cells. The development of perovskite-based tandem cells started in 2015 when the PCE of PSCs reached approximately 20% [211]. To date, significantly high PCEs obtained with triple-junction tandem cells such as InGaP/InGaAs/Ge have been utilized in space satellite missions. In the industry, the total cost of fabricating tandem solar cells, including materials and the process for stacking unit cells, becomes more than the cost of fabricating any single cell that constitutes the tandem structure. Apart from space applications, cost efficiency (efficiency-to-cost ratio) should be an essential issue in commercializing solar cells for consumers and for society in general. Therefore, it is desirable to boost the PCE by using tandem cells at no significant additional cost. For example, 20% more cost can be accepted for enhancing the PCE by 50%. However, a greater than 50% increase in cost may not be acceptable for a 50% increase in PCE, depending on the demand for the specific application. In this regard, a combination of cost-efficient perovskite and crystalline Si cells or a combination of two perovskite cells are promising candidates for tandem cell fabrication. Technically, the basic rule in the design of a tandem cell is to adjust the photocurrent density of each unit cell constituting the tandem to be equal to that of the other unit cells. For dual-junction tandem cells, the top cell with a larger bandgap that absorbs in the shorter wavelength region is adjusted to generate a photocurrent density that accurately matches the photocurrent density of the bottom cell produced by the light of the longer wavelength region, penetrating through the top cell. Such a current balance can be realized by tuning the bandgap of the top perovskite absorber, that is, the composition of halide perovskite. A simple method of making tandem cells is to mechanically superpose two solar cells that are independently fabricated using four terminals for electric combination. The advantage of these tandem cells is that the power generated by the top and bottom cells can be independently processed and combined electrically by the external circuitry so that the highest output is adjusted. However, the cost of the cell, which is the sum of two cells (four electrodes), becomes less efficient compared with the PCE of the tandem cell. Therefore, tandem cells with two terminals (two electrodes) are more desirable in terms of cost efficiency. Recent progress in perovskite-based tandem solar cells is summarized in review articles [212, 213]. Readers can also study theory and methods to enhance the efficiency of 2-terminal tandem cells, as described in Chapter 15. Theoretically, by sharing the solar spectrum (photon flux) with a perovskite top cell (E_g~1.6 eV) capable of a V_{OC} of 1.2 V and a crystalline Si bottom cell (E_g~1.1 eV) capable of a 0.8 V V_{OC}, the PCE of a perovskite/silicon

tandem cell can reach close to 30%, depending on the gain in V_{OC} and FF [214, 215]. Figure 1.18 shows an example of the layered structure of a perovskite/Si tandem cell and its solar spectrum absorption and photocurrent density divided by the top and bottom cells [216].

When a perovskite absorber of $Cs_{0.17}FA_{0.83}Pb(Br_{0.17}I_{0.83})_3$ (E_g of 1.63 eV) was employed with junction of an Si cell, this 2-terminal tandem cell achieved a PCE of 23.6% with a V_{OC} of 1.65 V [215]. Here, the top perovskite cell had an inverse structure, as depicted in Figure 1.18. The top layer was composed of PCBM as

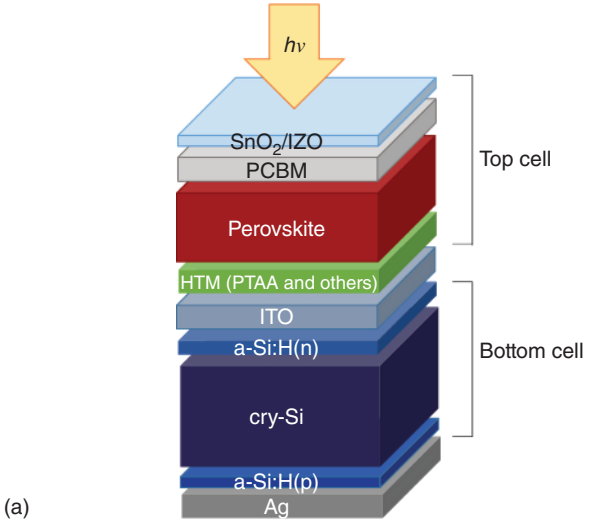

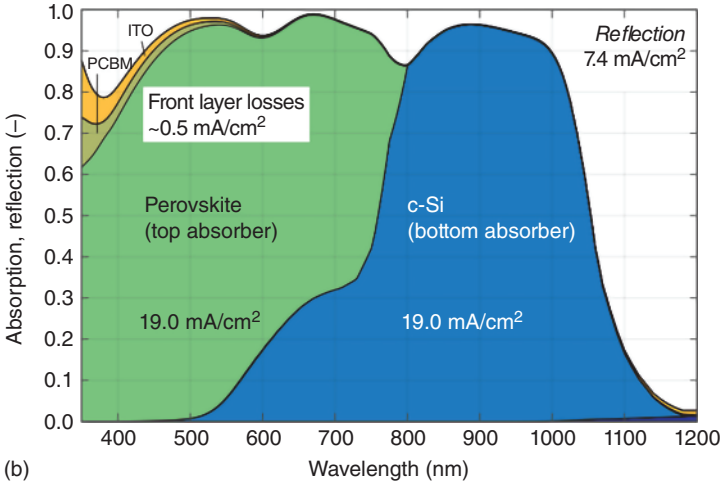

Figure 1.18 Layered structure of the stack of perovskite top cell and Si bottom cell in a 2-terminal tandem solar cell (a) and spectral light absorption performances and corresponding photocurrent densities of top and bottom cells (b). Source: Jäger et al. [216].

ETL and an ITO conductive layer as a transparent electrode. The perovskite top cell yielded a PCE close to 15%, which is lower than the efficiency obtained by the perovskite single cell due to the optical loss caused by the top semi-transparent electrode. Therefore, the optical transmittance of the top electrode, which must be prepared at a low temperature without damaging the perovskite, is key for ensuring a higher photocurrent in tandem cell performance. Duong et al. reported a PCE of 26.4% using a 4-terminal tandem cell with a mechanical stack of Rb-containing quadruple-cation perovskite (PCE of 17.4% with an E_g of 1.73 eV) and silicon cells (PCE of 23.9%) [217]. What rendered the PCE higher than the above 2-terminal cell was the higher PCE of the Si cell and the V_{OC} gain, which was 1.81 V (1.12 V for the top, 0.69 V for the bottom). In addition to the challenges of these studies, Oxford PV, a venture company, reported a certified PCE of 27.3% with a perovskite and crystalline Si tandem cell (active area was 1 cm^2). The PCE value achieved exceeds the top PCE of a single-junction Si cell (26.1%). In addition to these Si-based tandem designs, all perovskite-type tandem cells have been studied intensively due to their low-cost advantage. Huang and coworkers fabricated an all-perovskite tandem cell using $Cs_{0.4}FA_{0.6}PbI_{1.95}Br_{1.05}$ (E_g, 1.78 eV) and $Cs_{0.05}MA_{0.45}FA_{0.5}Pb_{0.5}Sn_{0.5}I_3$ (E_g, 1.21 eV) as the top and bottom cells, respectively, combined with SnO_{2-x} as the ETM and fullerene (C60) as the HTM. Achieving a V_{OC} of ~2.0 V and the highest PCE of 24.4%, the tandem cells could attain high stability, keeping efficiency almost unchanged for continuous 1-sun illumination for 1000 hours [218]. A certified PCE of 24.2% with a 1 cm^2 cell area was recently obtained by Nanjing University's group [219], who used a Pb–Sn mixed perovskite for bottom cells based on their previous work of passivating the Sn(II) against oxidation in achieving 24.8% PCE for a smaller device. Oxford PV mentions that the all-perovskite tandem cell is the most desirable junction of top and bottom cells in terms of their lowest cost of production and the feasibility of making tandem cells in the form of thin-film devices. In addition to these, top and bottom cells can have similar properties such as the lifetime of the device, light-soaking and thermal stabilities, and light intensity dependence of V_{OC} in power generation. With regard to intensity dependence, crystalline Si as the bottom cell shows characteristics quite different from that of the perovskite cell; the latter gives a relatively stable V_{OC} under low-intensity light, while the Si cell undergoes a large drop in V_{OC}. Furthermore, there is a large gap in the coefficient of thermal expansion between hybrid perovskite and inorganic Si, which can be an issue of long-term degradation of the tandem cell by thermal stress. Unlike existing semiconductor tandem cells, perovskite–perovskite tandem cells can be manufactured by printing technology using inks of source materials. A summary of the current progress in all-perovskite tandem cells was published including a comparison of progress in the certified efficiency between single cells and tandem cells as shown in Figure 1.19 [220].

In the industries, tandem cell fabrication is normally intended for outdoor use under sunlight. However, applications of tandem photovoltaic devices will include indoor power devices in IoT-related consumer electronics. Many manufacturers of perovskite-based photovoltaic devices aim to commercialize indoor devices for the IoT market, which is rapidly growing with the spread of wireless devices. These

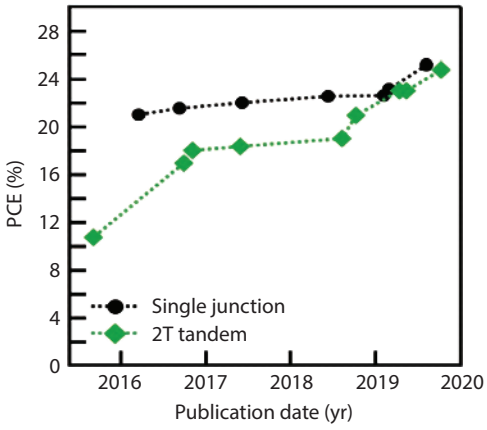

Figure 1.19 Certified PCEs of perovskite single-junction solar cells (black) and champion reported PCEs of monolithic 2-terminal (2T) all-perovskite tandems (green) as a function of publication date. Source: Moot et al. [220].

indoor power devices are required to have a lightweight body, if possible, with mechanical flexibility. By tuning the bandgaps of perovskite top and bottom cells, a perovskite-based thin-film tandem cell can be designed to have spectral sensitivity that can efficiently harvest illumination from LED lighting equipment and work with high output voltage. In the near future, it is expected that a thin flexible perovskite device with a plastic film substrate will be employed as a high-voltage power source in the IoT society.

1.9 Space Applications of the Perovskite Solar Cells

The state-of-the-art technologies of high-efficiency solar batteries have been applied to space satellite missions since 1958, where an American satellite Vanguard 1 was powered by Si solar cells. High-efficiency solar cells of crystalline Si and GaAs-based tandem structures are generally employed for satellite solar cell modules. In 2015, our group had the first meeting with a research team of Japan Aerospace Exploration Agency (JAXA), who had been searching for next-generation new solar cells that can satisfy the conditions of high PCE of over 20%, along with being lightweight and cost-effective as compared with Si. They chose perovskite solar cells (PSCs) as the target of examination because the lightweight flexibility of the module is regarded as feasible for future development. The central goal of examination is to assess the stability of PSCs against the harsh environments of space. In fact, most commercial solar cells show degradation of materials in the space environment mainly due to the energetic particle irradiations such as electron and proton beams. Therefore, all devices loaded on satellites should have robust stability against continuous exposure to high-energy space irradiations. In addition to these irradiations, solar cells are continuously exposed to sunlight, which can heat the device up to 100 °C. In collaboration with JAXA, we conducted an examination of space irradiation tolerance of PSCs as a laboratory simulation using high-energy electron and proton particle beams. It is expected that the defect-tolerant nature of organo-lead halide

perovskite semiconductors enables PSCs to survive under high-energy irradiation on perovskite films. Several studies have reported the relatively high stability of perovskite materials ($MAPbI_3$) against proton irradiation of particle energy tuned at 68 MeV [221, 223]. We investigated the particle irradiation tolerance of $MAPbI_3$ and mixed-cation/halide perovskite absorbers and evaluated the stability of their solar cells. Before conducting irradiation experiments, the thermal stability of perovskite devices was tested by keeping the device at high and low temperatures of 100 and −80 °C, which correspond to the satellite orbit with and without sunlight, respectively. This test revealed the fragility of organic HTMs instead of the perovskite absorber. Spiro-OMeTAD deteriorated very quickly at 100 °C while a polymer conductor, P3HT, as HTM survived by maintaining the V_{OC} of the cell. In proton and electron irradiation, it was found that both $MAPbI_3$ and mixed-cation PSCs using P3HT HTM have a fairly high tolerance to high fluence and large doses of protons (50 keV) and electrons (1 MeV), which can destroy crystalline Si and GaAs-based solar cells [224]. Figure 1.20 shows how PSCs are tolerant to proton irradiation fluence, up to 10^{14} particles per cm^2. Such robust durability of perovskite cells is enabled by using very thin absorber films (for visible light conversion), which permit the penetration of high-energy particles without causing collision damage. In addition, our recent investigation using 1 MeV electron irradiation to triple cation perovskite ($Cs_{0.05}(MA_{0.17}FA_{0.83})_{0.95}Pb(I_{0.93}Br_{0.07})_3$) elucidated that the irradiation gives a low damage to the carrier diffusion lengths as confirmed by PL measurements and the device showed no degradation in performance (J_{sc}, V_{OC}, PCE) at a high fluence of 1×10^{16} electrons/cm^2 [222]. Obviously, the defect tolerance property of perovskite semiconductors greatly contributes to such rare performance in a space environment.

The radiation tolerance of lead halide perovskites and their solar cells has been confirmed by other research groups. Accordingly, the future applications of PSCs to durable power sources in space satellite missions are promising. A monolithic perovskite/copper indium gallium selenide (CIGS) tandem solar cell as a thin and lightweight power source was designed by Lang et al. using $[Cs_{0.05}(MA_{0.17}FA_{0.83})_{0.95}]Pb(I_{0.83}Br_{0.17})_3$ as the perovskite absorber. This tandem cell had a PCE of 18.0% at air mass (AM) 1.5 (15.1% at AM0) and a specific power per weight of 2.1 W/g, which is ∼3 times larger than those of typically used GaInP/GaAs/Ge absorbers at 0.8 W/g. In radiation tolerance tests, the cells achieved high durability against high-energy proton irradiation (68 MeV) by retaining over 85% of their initial PCE at a dose of 2×10^{12} cm^{-2} [225]. The same group reported the radiation hardness of $MAPbI_3$ against the same proton beam and the self-healing ability of the perovskite after proton irradiation [221]. The first trial of mounting a PSC on a space rocket was conducted in June 2019 by a German group in collaboration with the German Aerospace Center [226]. The suborbital rocket flight reached an altitude of approximately 240 km (low-Earth orbit) above the surface. Exposing the perovskite cells comprising perovskite of $MA_{0.17}FA_{0.83}Pb(I_{0.17}Br_{0.83})_3$, spiro-OMeTAD HTM, and TiO_2 or SnO_2 ETM to near-space AM0 sunlight, including strong UV light, produced a power corresponding to a PCE of approximately 14%. In this trial, more experiments will be planned

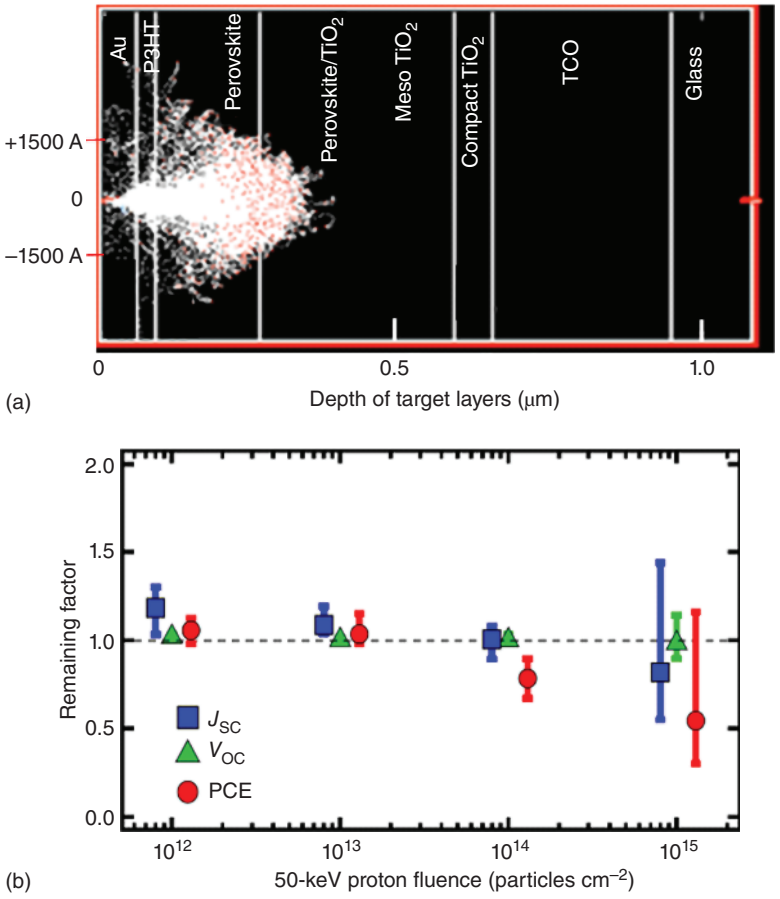

Figure 1.20 Profile of 50 keV proton beam penetration depth along the depth of the multilayered structure in the MA perovskite cell determined using SRIM/TRIM (stopping and range of ions in matter/transport of ions in matter) analysis [224] (a), indicating proton-induced collision damage is focused on the perovskite layer. Proton irradiation tolerance of mixed-cation/halide perovskite cells (b) showing changes of J_{SC}, V_{OC}, P_{max}, and PCE plotted against proton fluence. Source: Miyazawa et al. [224].

for possible applications of PSCs in deep-space missions where strong proton and electron radiations exist.

1.10 Conclusion and Perspectives

Rare photophysical properties of metal halide perovskites have led to the emergence of many research topics in fundamental science related to organic–inorganic hybrid ionic semiconductors and have simultaneously inspired various types of device applications in engineering. Both fundamental and applied research proceed by taking highly interdisciplinary approaches; material synthesis is mostly

a solution-based chemical process while the characterization of perovskite semiconductors requires physical methods and device fabrication involves chemistry, physics, and electronics. Therefore, efficient collaboration between different disciplines can accelerate research outcomes. In industrial applications, the solution (ink)-based printing process used in the manufacture of thin perovskite films is a tremendous advantage in terms of high-throughput and low-cost coating processes enabling roll-to-roll manufacturing of flexible modules. The high level of defect tolerance endowed to the perovskite materials, as reflected by the long lifetimes of photoexcited free carriers, plays a central role in realizing high performance of optoelectronic devices. This leads to a high voltage output in photovoltaic power generation, which can be compared with the best photovoltaic performance obtained by GaAs. High-voltage performance becomes especially advantageous when the perovskite device is used as an indoor power source in IoT applications where IoT devices and their secondary batteries (Li-ion batteries, etc.) require higher voltage input under weak light to drive the circuitry. One of the goals of perovskite photovoltaics is to achieve the excellent photophysical properties of GaAs semiconductors, which exhibit an open-circuit voltage and PCE close to the SQ limits with a bandgap of 1.42 eV at the absorption edge of nearby 900 nm, the optimum wavelength for a single-junction cell to harvest the power of solar irradiation. To ensure this bandgap, lead must be fully or partially replaced with other metals of group 14 or 15. Presently, Sn(II)-based perovskites are the most promising candidates, although their low stability against oxidation is the main issue for practical applications. Based on the top efficiency of PSCs (25.5%), the efficiency of perovskite modules for practical use is expected to reach more than 22%, which is considered sufficient for commercial devices in terms of cost performance. The major issue of commercialization has been the stability and durability of the module. However, this is being addressed by developing durable compositions and passivation methods in addition to encapsulation technology. Another issue is ensuring the environmental safety of materials. In the future, lead will be the subject of total replacement with other metals such as Sn, Bi, Sb, Ag, etc. Efforts to change the perovskite composition and improve the film morphology have so far indicated difficulty in engineering to achieve sufficiently high device performance, although theoretical models predict the high potential of photovoltaic functions. However, more studies will be done to pioneer new compositions (perovskite or non-perovskite) and methods of crystalline film formation based on chemical engineering. If we look at applications other than photovoltaics, many these including LED, photodetectors, and lasers are progressing, and halide perovskite science and engineering are expected to continue to develop significantly in the future.

References

1 Kojima, A., Teshima, K., Shirai, Y., and Miyasaka, T. (2009). Organometal halide perovskites as visible-light sensitizers for photovoltaic cells. *J. Am. Chem. Soc.* 131: 6050–6051.

2 National Renewable Energy Laboratory (2021). Research Cell Record Efficiency Chart. Best Research-Cell Efficiencies. https://www.nrel.gov/pv/cell-efficiency.html https://http://www.nrel.gov/pv/assets/pdfs/best-research-cell-efficiencies.20190802.pdf(accessed 23 July 2021).

3 Jena, A.K., Kulkarni, A., and Miyasaka, T. (2019). Halide perovskite photovoltaics: background, status, and future prospects. *Chem. Rev.* 119: 3036–3103.

4 Farnell, G.C. and Chanter, J.B. (1961). The quantum sensitivity of photographic emulsion grains. *J. Photogr. Sci.* 9: 73–83.

5 Attridge, G.G. (1982). A contribution to interpretation of the photographic characteristic curve. *J. Photogr. Sci.* 30: 197–207.

6 Tao, S.X., Cao, X., and Bobbert, P.A. (2017). Accurate and efficient band gap predictions of metal halide perovskites using DFT-1/2 methods: GW accuracy with DFT expense. *Sci. Rep.* 7: 14386.

7 Tubbs, M.R. and Forty, A.J. (1964). Photographic applications of lead iodide. *Br. J. Appl. Phys.* 15: 1553–1558.

8 Kojima, A., Teshima, K., Miyasaka, T. and Shirai, Y. (2006). Novel photoelectrochemical cell with mesoscopic electrodes sensitized by lead-halide compounds (2). *The Electrochemical Society (ECS), 210th Meeting Abstracts*, MA2006-02 397.

9 Lee, M.M., Teuscher, J., Miyasaka, T. et al. (2012). Efficient hybrid solar cells based on meso-superstructured organometal halide perovskites. *Science* 338: 643–647.

10 Miyasaka, T. (2018). Lead halide perovskites in thin film photovoltaics: background and perspectives. *Bull. Chem. Soc. Jpn.* 91: 1058–1068.

11 Kojima, A., Ikegami, M., Teshima, K., and Miyasaka, T. (2012). Highly luminescent lead bromide perovskite nanoparticles synthesized with porous alumina media. *Chem. Lett.* 41: 397–399.

12 Rose, G. (1839). Beschreibung einiger neuen Mineralien des Urals. *Ann. Phys. Chem.* 124: 551–573.

13 Chakhmouradian, A.R. and Woodward, P.M. (2014). Celebrating 175 years of Perovskite research: a tribute to Roger H. Mitchell. *Phys. Chem. Miner.* 41: 387–391.

14 Dirin, D.N., Cherniukh, I., Yakunin, S. et al. (2016). Solution-grown $CsPbBr_3$ perovskite single crystals for photon detection. *Chem. Mater.* 28: 8470–8474.

15 Katz, E.A. (2020). Perovskite: name puzzle and German-Russian odyssey of discovery. *Helv. Chim. Acta* 103: e2000061.

16 Goldschmidt, V.M. (1926). Die Gesetze der Krystallochemie. *Die Naturwiss.* 21: 477–485.

17 Acosta, M., Novak, N., Rojas, V. et al. (2017). $BaTiO_3$-based piezoelectrics: fundamentals, current status, and perspectives. *Appl. Phys. Rev.* 4: 041305.

18 Yuan, Y., Xiao, Z., Yang, B., and Huang, J. (2014). Arising applications of ferroelectric materials in photovoltaic devices. *J. Mater. Chem. A* 2: 6027–6041.

19 Wells, H.L. (1893). Über die cäsium- und kalium-bleihalogenide. *Z. Anorg. Chem.* 3: 195–210.

20 Møller, C.K. (1957). A phase transition in cæsium plumbochloride. *Nature* 180: 981–982.

21 Møller, C.K. (1957). Crystal structure and photoconductivity of cæsium plumbohalides. *Nature* 182: 1436.

22 Weber, D. (1978). $CH_3NH_3PbX_3$, ein Pb (II)-system mit kubischer perowskitstruktur / $CH_3NH_3PbX_3$, a Pb(II)-system with cubic perovskite structure. *Z. Naturforsch., B* 33: 1443–1445.

23 Weber, D. (1978). $CH_3NH_3SnBr_xI_{3-x}$ (x = 0-3), ein Sn (II)-system mit kubischer perowskitstruktur / $CH_3NH_3SnBr_xI_{3-x}$(x = 0-3), a Sn(II)-system with cubic perovskite structure. *Z. Naturforsch., B* 33: 862–865.

24 Mitzi, D.B. (1999). Synthesis, structure, and properties of organic-inorganic perovskites and related materials. Progress in inorganic chemistry. *Progress in Inorganic Chemistry* 48: 1–122.

25 Mitzi, D.B. (2000). Organic–inorganic perovskites containing trivalent metal halide layers: the templating influence of the organic cation layer. *Inorg. Chem.* 39: 6107–6113.

26 Era, M. and Oka, S. (2000). PbBr-based layered perovskite film using the langmuir–Blodgett technique. *Thin Solid Films* 376: 232–235.

27 Takeoka, Y., Asai, K., Rikukawa, M., and Sanui, K. (2001). Incorporation of conjugated polydiacetylene systems into organic–inorganic quantum-well structures. *Chem. Commun.*: 2592–2593.

28 Kondo, T., Iwamoto, S., Hayase, S. et al. (1998). Resonant third-order optical nonlinearity in the layered perovskite-type material $(C_6H_{13}NH_3)_2PbI_4$. *Solid State Commun.* 105: 503–506.

29 Tanaka, K. and Kondo, T. (2003). Bandgap and exciton binding energies in lead-iodide-based natural quantum-well crystals. *Sci. Technol. Adv. Mater.* 4: 599–604.

30 Ema, K., Umeda, K., Toda, M. et al. (2006). Huge exchange energy and fine structure of excitons in an organic-inorganic quantum well material. *Phys. Rev. B* 73: 241310-1-4.

31 Ishi, J., Mizuno, M., Kunugita, H. et al. (1998). Third-order optical nonlinearity due to excitons and biexcitons in a self-organized quantum-well material $(C_6H_{13}NH_3)_2PbI_4$. *J. Nonlinear Opt. Phys. Mater.* 07: 153–159.

32 Miyasaka, T., Ikegami, M., and Kijitori, Y. (2007). Photovoltaic performance of plastic dye-sensitized electrodes prepared by low-temperature binder-free coating of mesoscopic titania. *J. Electrochem. Soc.* 154: A455–A461.

33 Ikeda, N., Teshima, K., and Miyasaka, T. (2006). Conductive polymer–carbon–imidazolium composite: a simple means for constructing solid-state dye-sensitized solar cells. *Chem. Commun.*: 1733–1735.

34 Miyasaka, T. (2011). Toward printable sensitized mesoscopic solar cells: light-harvesting management with thin TiO_2 films. *J. Phys. Chem. Lett.* 2: 262–269.

35 Kojima, A., Teshima, K., Shirai, Y., and Miyasaka, T. (2008). Novel photoelectrochemical cell with mesoscopic electrodes sensitized by lead-halide

compounds (11). *The Electrochemical Society (ECS), 214th Meeting (PRiME. 2008), Abstracts*, MA2008-2, 27. A.

36 Miyasaka, T. (2015). Perovskite photovoltaics: rare functions of organo lead halide in solar cells and optoelectronic devices. *Chem. Lett.* 44: 720–729.

37 Im, J.H., Lee, C.R., Lee, J.W. et al. (2011). 6.5% efficient perovskite quantum-dot-sensitized solar cell. *Nanoscale* 3: 4088–4093.

38 Murakami, T.N., Ito, S., Wang, Q. et al. (2006). Highly efficient dye-sensitized solar cells based on carbon black counter electrodes. *J. Electrochem. Soc.* 153: A2255–A2261.

39 Snaith, H.J., Petrozza, A., Ito, S. et al. (2009). Charge generation and photovoltaic operation of solid-state dye-sensitized solar cells incorporating a high extinction coefficient indolene-based sensitizer. *Adv. Funct. Mater.* 19: 1810–1818.

40 Stranks, S.D., Eperon, G.E., Grancini, G. et al. (2013). Electron-hole diffusion lengths exceeding 1 micrometer in an organometal trihalide perovskite absorber. *Science* 342: 341–342.

41 Wehrenfennig, C., Eperon, G.E., Johnston, M.B. et al. (2013). High charge carrier mobilities and lifetimes in organolead trihalide perovskites. *Adv. Mater.* 26: 1584–1589.

42 Dong, Q., Fang, Y., Shao, Y. et al. (2015). Electron-hole diffusion lengths >175 μm in solution-grown $CH_3NH_3PbI_3$ single crystals. *Science* 347: 967–969.

43 Jeong, M., Choi, I.W., Go, E.M. et al. (2020). Stable perovskite solar cells with efficiency exceeding 24.8% and 0.3-V voltage loss. *Science* 369: 1615–1620.

44 Kim, G., Min, H., Lee, K.S. et al. (2020). Impact of strain relaxation on performance of α-formamidinium lead iodide perovskite solar cells. *Science* 370: 108–112.

45 Wang, H., Guerrero, A., Bou, A. et al. (2019). Kinetic and material properties of interfaces governing slow response and long timescale phenomena in perovskite solar cells. *Energy Environ. Sci.* 12: 2054–2079.

46 Suarez, B., Gonzalez-Pedro, V., Ripolles, T.S. et al. (2014). Recombination study of combined halides (Cl, Br, I) perovskite solar cells. *J. Phys. Chem. Lett.* 5: 1628–1635.

47 Eperon, G.E., Stranks, S.D., Menelaou, C. et al. (2014). Formamidinium lead trihalide: a broadly tunable perovskite for efficient planar heterojunction solar cells. *Energy Environ. Sci.* 7: 982–988.

48 Miyano, K., Tripathi, N., Yanagida, M., and Shirai, Y. (2016). Lead halide perovskite photovoltaic as a model p–i–n diode. *Acc. Chem. Res.* 49: 303–310.

49 Brivio, F., Butler, K.T., Walsh, A., and Schilfgaarde, M. (2014). Relativistic quasiparticle self-consistent electronic structure of hybrid halide perovskite photovoltaic absorbers. *Phys. Rev. B* 89: 155204.

50 Tanaka, K., Takahashi, T., Ban, T. et al. (2003). Comparative study on the excitons in lead-halide-based perovskite-type crystals $CH_3NH_3PbBr_3$ $CH_3NH_3PbI_3$. *Solid State Commun.* 127: 619–623.

51 Yin, W.J., Shi, T., and Yan, Y. (2015). Superior photovoltaic properties of lead halide perovskites: insights from first-principles theory. *J. Phys. Chem. C* 119: 5253–5264.

52 Green, M.A., Ho-Baillie, A., and Snaith, H.J. (2014). The emergence of perovskite solar cells. *Nat. Photonics* 8: 506–514.

53 Giorgi, G., Fujisawa, J.I., Segawa, H., and Yamashita, K. (2013). Small photocarrier effective masses featuring ambipolar transport in methylammonium lead iodide perovskite: a density functional analysis. *J. Phys. Chem. Lett.* 4: 4213–4216.

54 De Quilettes, D.W., Vorpahl, S.M., Stranks, S.D. et al. (2015). Impact of microstructure on local carrier lifetime in perovskite solar cells. *Science* 348: 683–686.

55 Stranks, S.D. and Snaith, H.J. (2015). Metal-halide perovskites for photovoltaic and light-emitting devices. *Nat. Nanotechnol.* 10: 391–402.

56 Liu, Z., Krückemeier, L., Krogmeier, B. et al. (2019). Open-circuit voltages exceeding 1.26 V in planar methylammonium lead iodide perovskite solar cells. *ACS Energy Lett.* 4: 110–117.

57 Shockley, W. and Queisser, H.J. (1961). Detailed balance limit of efficiency of p-n junction solar cells. *J. Appl. Phys.* 32: 510–519.

58 Sha, W.E.I., Ren, X., Chen, L., and Choy, W.C.H. (2015). The efficiency limit of $CH_3NH_3PbI_3$ perovskite solar cells. *Appl. Phys. Lett.* 106: 221104.

59 Shi, D., Adinolfi, V., Comin, R. et al. (2015). Low trap-state density and long carrier diffusion in organolead trihalide perovskite single crystals. *Science* 347: 519–522.

60 Stranks, S.D., Burlakov, V.M., Leijtens, T. et al. (2014). Recombination kinetics in organic-inorganic perovskites: excitons, free charge, and subgap states. *Phys. Rev. Appl.* 2: 034007.

61 Bi, D., Tress, W., Dar, M.I. et al. (2016). Efficient luminescent solar cells based on tailored mixed-cation perovskites. *Sci. Adv.* 2: e1501170 (1-7).

62 Kim, G.M., Ishii, A., Öz, S., and Miyasaka, T. (2019). MACl-assisted Ge doping of Pb-hybrid perovskite: a universal route to stabilize high performance perovskite solar cells. *Adv. Energy Mater.* 10 1903299, 1–8.

63 Tress, W., Marinova, N., Inganäs, O. et al. (2014). Predicting the open-circuit voltage of $CH_3NH_3PbI_3$ perovskite solar cells using electroluminescence and photovoltaic quantum efficiency spectra: the role of radiative and non-radiative recombination. *Adv. Energy Mat.* 5: 1400812.

64 Tvingstedt, K., Malinkiewicz, O., Baumann, A. et al. (2014). Radiative efficiency of lead iodide based perovskite solar cells. *Sci. Rep.* 4: 6071.

65 Correa Baena, J.P., Steier, L., Tress, W. et al. (2015). Highly efficient planar perovskite solar cells through band alignment engineering. *Energy Environ. Sci.* 8: 2928–2934.

66 Saliba, M., Matsui, T., Seo, J.-Y. et al. (2016). Cesium-containing triple cation perovskite solar cells: improved stability, reproducibility and high efficiency. *Energy Environ. Sci.* 9: 1989–1997.

67 Singh, T., Öz, S., Sasinska, A. et al. (2018). Sulfate-assisted interfacial engineering for high yield and efficiency of triple cation perovskite solar cells with alkali-doped TiO_2 electron-transporting layers. *Adv. Funct. Mater* 28: 1706287–1706296.

68 Kim, G.M., Ishii, A., Ohkura, Y., Sato, H., and Miyasaka. T. (2021). in preparation.

69 Guo, Z., Jena, A.K., Takei, I. et al. (2020). V_{OC} over 1.4 V for amorphous tin-oxide-based dopant-free $CsPbI_2Br$ perovskite solar cells. *J. Am. Chem. Soc.* 142: 9725–9734.

70 Xing, G., Mathews, N., Sun, S. et al. (2013). Long-range balanced electron- and hole-transport lengths in organic-inorganic $CH_3NH_3PbI_3$. *Science* 342: 344–347.

71 Bi, Y., Hutter, E.M., Fang, Y. et al. (2016). Charge carrier lifetimes exceeding 15 μs in methylammonium lead iodide single crystals. *J. Phys. Chem. Lett.* 7: 923–928.

72 Chouhan, A.S., Jasti, N.P., Hadke, S. et al. (2017). Large grained and high charge carrier lifetime $CH_3NH_3PbI_3$ thin-films: implications for perovskite solar cells. *Curr. Appl. Phys.* 17: 1335–1340.

73 Johnston, M.B. and Herz, L.M. (2016). Hybrid perovskites for photovoltaics: charge-carrier recombination, diffusion, and radiative efficiencies. *Acc. Chem. Res.* 49: 146–154.

74 Ponseca, C.S., Savenije, T.J., Abdellah, M. et al. (2014). Organometal halide perovskite solar cell materials rationalized: ultrafast charge generation, high and microsecond-long balanced mobilities, and slow recombination. *J. Am. Chem. Soc.* 136: 5189–5192.

75 Smecca, E., Numata, Y., Deretzis, I. et al. (2016). Stability of solution-processed $MAPbI_3$ and $FAPbI_3$ layers. *Phys. Chem. Chem. Phys.* 18: 13413–13422.

76 Turren-Cruz, S.H., Hagfeldt, A., and Saliba, M. (2018). Methylammonium-free, high-performance, and stable perovskite solar cells on a planar architecture. *Science* 362: 449–453.

77 Miyasaka, T., Kulkarni, A., Kim, G.M. et al. (2019). Perovskite solar cells: can we go organic-free, lead-free, and dopant-free? *Adv. Energy Mater.* 10, 1902500, 1–20.

78 Hoefler, S.F., Trimmel, G., and Rath, T. (2017). Progress on lead-free metal halide perovskites for photovoltaic applications: a review. *Monatsh. Chem. Chem. Mon.* 148: 795–826.

79 Ono, L.K., Juarez-Perez, E.J., and Qi, Y. (2017). Progress on perovskite materials and solar cells with mixed cations and halide anions. *ACS Appl. Mater. Interfaces* 9: 30197–30246.

80 Kubicki, D.J., Prochowicz, D., Hofstetter, A. et al. (2017). Phase segregation in Cs-, Rb- and K-doped mixed-cation $(MA)_x(FA)_{1-x}PbI_3$ hybrid perovskites from solid-state NMR. *J. Am. Chem. Soc.* 139: 14173–14180.

81 Jacobsson, T.J., Svanström, S., Andrei, V. et al. (2018). Extending the compositional space of mixed lead halide perovskites by Cs, Rb, K, and Na doping. *J. Phys. Chem. C* 122: 13548–13557.

82 Chen, Q., De Marco, N., Yang, Y. et al. (2015). Under the spotlight: the organic–inorganic hybrid halide perovskite for optoelectronic applications. *Nano Today* 10: 355–396.

83 Akin, S., Akman, E., and Sonmezoglu, S. (2020). $FAPbI_3$-based perovskite solar cells employing hexyl-based ionic liquid with an efficiency over 20% and excellent long-term stability. *Adv. Funct. Mater.* 30: 2002964.

84 Jeon, N.J., Noh, J.H., Yang, W.S. et al. (2015). Compositional engineering of perovskite materials for high-performance solar cells. *Nature* 517: 476–480.

85 Binek, A., Hanusch, F.C., Docampo, P., and Bein, T. (2015). Stabilization of the trigonal high-temperature phase of formamidinium lead iodide. *J. Phys. Chem. Lett.* 6: 1249–1253.

86 Leijtens, T., Bush, K., Cheacharoen, R. et al. (2017). Towards enabling stable lead halide perovskite solar cells; interplay between structural, environmental, and thermal stability. *J. Mater. Chem. A* 5: 11483–11500.

87 Niu, G., Li, W., Li, J. et al. (2017). Enhancement of thermal stability for perovskite solar cells through cesium doping. *RSC Adv.* 7: 17473–17479.

88 Li, Z., Yang, M., Park, J.S. et al. (2016). Stabilizing perovskite structures by tuning tolerance factor: formation of formamidinium and cesium lead iodide solid-state alloys. *Chem. Mater.* 28: 284–292.

89 Yi, C., Luo, J., Meloni, S. et al. (2016). Entropic stabilization of mixed a-cation ABX_3 metal halide perovskites for high performance perovskite solar cells. *Energy Environ. Sci.* 9: 656–662.

90 Richardson, G., O'Kane, S.E.J., Niemann, R.G. et al. (2016). Can slow-moving ions explain hysteresis in the current–voltage curves of perovskite solar cells? *Energy Environ. Sci.* 9: 1476–1485.

91 Zhang, Y., Liu, M., Eperon, G.E. et al. (2015). Charge selective contacts, mobile ions and anomalous hysteresis in organic–inorganic perovskite solar cells. *Mater. Horiz.* 2: 315–322.

92 Ravishankar, S., Almora, O., Echeverría-Arrondo, C. et al. (2017). Surface polarization model for the dynamic hysteresis of perovskite solar cells. *J. Phys. Chem. Lett.* 8: 915–921.

93 Calado, P., Telford, A.M., Bryant, D. et al. (2016). Evidence for ion migration in hybrid perovskite solar cells with minimal hysteresis. *Nat. Commun.* 7: 13831 (1-10).

94 Weber, S.A.L., Hermes, I.M., Turren-Cruz, S.H. et al. (2018). How the formation of interfacial charge causes hysteresis in perovskite solar cells. *Energy Environ. Sci.* 11: 2404–2413.

95 Almosni, S., Cojocaru, L., Li, D. et al. (2017). Tunneling-assisted trapping as one of the possible mechanisms for the origin of hysteresis in perovskite solar cells. *Energy Technol.* 5: 1767–1774.

96 Singh, T. and Miyasaka, T. (2017). Stabilizing the efficiency beyond 20% with a mixed cation perovskite solar cell fabricated in ambient air under controlled humidity. *Adv. Energy Mater.* 8: 1700677 (1-9).

97 Saliba, M., Matsui, T., Domanski, K. et al. (2016). Incorporation of rubidium cations into perovskite solar cells improves photovoltaic performance. *Science* 354: 206–209.

98 Hu, Y., Hutter Eline, M., Rieder, P. et al. (2018). Understanding the role of cesium and rubidium additives in perovskite solar cells: trap states, charge transport, and recombination. *Adv. Energy Mater.* 8: 1703057 (1-11).

99 Han, G., Hadi, H.D., Bruno, A. et al. (2018). Additive selection strategy for high performance perovskite photovoltaics. *J. Phys. Chem. C* 122: 13884–13893.

100 Brunetti, B., Cavallo, C., Ciccioli, A. et al. (2016). On the thermal and thermodynamic (in)stability of methylammonium lead halide perovskites. *Sci. Rep.* 6: 31896 (1-12).

101 Arora, N., Dar, M.I., Hinderhofer, A. et al. (2017). Perovskite solar cells with CuSCN hole extraction layers yield stabilized efficiencies greater than 20%. *Science* 358: 768–771.

102 Shi, L., Bucknall, M.P., Young, T.L. et al. (2020). Gas chromatography–mass spectrometry analyses of encapsulated stable perovskite solar cells. *Science* 368: eaba2412.

103 Wang, R., Mujahid, M., Duan, Y. et al. (2019). A review of perovskites solar cell stability. *Adv. Funct. Mater.* 29: 1808843.

104 Eames, C., Frost, J.M., Barnes, P.R.F. et al. (2015). Ionic transport in hybrid lead iodide perovskite solar cells. *Nat. Commun.* 6: 7497 (1-8).

105 Yuan, Y., Wang, Q., Shao, Y. et al. (2015). Electric-field-driven reversible conversion between methylammonium lead triiodide perovskites and lead iodide at elevated temperatures. *Adv. Energy Mater.* 6: 1501803 (1-7).

106 Minns, J.L., Zajdel, P., Chernyshov, D. et al. (2017). Structure and interstitial iodide migration in hybrid perovskite methylammonium lead iodide. *Nat. Commun.* 8: 15152 (1-5).

107 Yuan, Y., Chae, J., Shao, Y. et al. (2015). Photovoltaic switching mechanism in lateral structure hybrid perovskite solar cells. *Adv. Energy Mater.* 5: 1500615 (1-7).

108 Wu, T., Ahmadi, M., and Hu, B. (2018). Giant current amplification induced by ion migration in perovskite single crystal photodetectors. *J. Mater. Chem. C* 6: 8042–8050.

109 Luo, Y., Khoram, P., Brittman, S. et al. (2017). Direct observation of halide migration and its effect on the photoluminescence of methylammonium lead bromide perovskite single crystals. *Adv. Mater.* 29: 1703451 (1-7).

110 Leguy, A.M.A., Hu, Y., Campoy-Quiles, M. et al. (2015). Reversible hydration of $CH_3NH_3PbI_3$ in films, single crystals, and solar cells. *Chem. Mater.* 27: 3397–3407.

111 Habisreutinger, S.N., Leijtens, T., Eperon, G.E. et al. (2014). Carbon nanotube/polymer composites as a highly stable hole collection layer in perovskite solar cells. *Nano Lett.* 14: 5561–5568.

112 Chaudhary, B., Kulkarni, A., Jena, A.K. et al. (2017). Poly(4-vinylpyridine)-based interfacial passivation to enhance voltage and

moisture stability of lead halide perovskite solar cells. *ChemSusChem* 10: 2473–2479.

113 Hou, Y., Zhou, Z.R., Wen, T. et al. (2019). Enhanced moisture stability of metal halide perovskite solar cells based on sulfur-oleylamine surface modification. *Nanoscale Horiz.* 4: 208–213.

114 Abdelmageed, G., Sully, H.R., Bonabi Naghadeh, S. et al. (2018). Improved stability of organometal halide perovskite films and solar cells toward humidity via surface passivation with oleic acid. *ACS Appl. Energy Mater.* 1: 387–392.

115 Cao, J., Li, C., Lv, X. et al. (2018). Efficient grain boundary suture by low-cost tetra-ammonium zinc phthalocyanine for stable perovskite solar cells with expanded photoresponse. *J. Am. Chem. Soc.* 140: 11577–11580.

116 Zhang, F., Lu, H., Tong, J. et al. (2020). Advances in two-dimensional organic–inorganic hybrid perovskites. *Energy Environ. Sci.* 13: 1154–1186.

117 Smith, I.C., Hoke, E.T., Solis-Ibarra, D. et al. (2014). I. A layered hybrid perovskite solar-cell absorber with enhanced moisture stability. *Angew. Chem.* 126: 11414–11417.

118 Cao, D.H., Stoumpos, C.C., Farha, O.K. et al. (2015). 2D homologous perovskites as light-absorbing materials for solar cell applications. *J. Am. Chem. Soc.* 137: 7843–7850.

119 Etgar, L. (2018). The merit of perovskite's dimensionality; can this replace the 3D halide perovskite? *Energy Environ. Sci.* 11: 234–242.

120 Wang, Z., Lin, Q., Chmiel, F.P. et al. (2017). Efficient ambient-air-stable solar cells with 2D–3D heterostructured butylammonium-caesium-formamidinium lead halide perovskites. *Nat. Energy* 2: 17135.

121 Lu, J., Jiang, L., Li, W. et al. (2017). Diammonium and monoammonium mixed-organic-cation perovskites for high performance solar cells with improved stability. *Adv. Energy Mater.* 7: 1700444 (1-10).

122 Ye, J., Zheng, H., Zhu, L. et al. (2017). Enhanced moisture stability of perovskite solar cells with mixed-dimensional and mixed-compositional light-absorbing materials. *Solar RRL* 1: 1700125 (1-8).

123 Li, N., Zhu, Z., Chueh, C.C. et al. (2016). Mixed cation $FA_xPEA_{1-x}PbI_3$ with enhanced phase and ambient stability toward high-performance perovskite solar cells. *Adv. Energy Mater.* 7: 1601307 (1-9).

124 Hu, R., Zhang, Y., Paek, S. et al. (2020). Enhanced stability of α-phase $FAPbI_3$ perovskite solar cells by insertion of 2D $(PEA)_2PbI_4$ nanosheets. *J. Mater. Chem. A* 8: 8058–8064.

125 Chen, P., Bai, Y., Wang, S. et al. (2018). In situ growth of 2D perovskite capping layer for stable and efficient perovskite solar cells. *Adv. Funct. Mat.* 28: 1706923.

126 Xu, H., Sun, Y., Zheng, H. et al. (2019). High-performance and moisture-stable perovskite solar cells with a 2D modified layer via introducing a high dipole moment cation. *J. Mater. Chem. C.* 7: 15276–15284.

127 Chen, M., Li, P., Liang, C. et al. (2020). Enhanced efficiency and stability of perovskite solar cells by 2D perovskite vapor-assisted interface optimization. *J. Energy Chem.* 45: 103–109.

128 Mei, A., Li, X., Liu, L. et al. (2014). A hole-conductor–free, fully printable mesoscopic perovskite solar cell with high stability. *Science* 345: 295–298.

129 Grancini, G., Roldán-Carmona, C., Zimmermann, I. et al. (2017). One-year stable perovskite solar cells by 2D/3D. *Nat. Commun.* 8: 15684.

130 Liu, X., Zhang, Y., Hua, J. et al. (2018). Improving the intrinsic thermal stability of the $MAPbI_3$ perovskite by incorporating cesium 5-aminovaleric acetate. *RSC Adv.* 8: 14991–14994.

131 Fagiolari, L. and Bella, F. (2019). Carbon-based materials for stable, cheaper, and large-scale processable perovskite solar cells. *Energy Environ. Sci.* 12: 3437–3472.

132 Yavari, M., Mazloum-Ardakani, M., Gholipour, S. et al. (2018). Reducing surface recombination by a poly(4-vinylpyridine) interlayer in perovskite solar cells with high open-circuit voltage and efficiency. *ACS Omega* 3: 5038–5043.

133 Zong, Y., Zhou, Y., Zhang, Y. et al. (2018). Continuous grain-boundary functionalization for high-efficiency perovskite solar cells with exceptional stability. *Chem* 4: 1404–1415.

134 Fang, H.H., Adjokatse, S., Wei, H. et al. (2016). Ultrahigh sensitivity of methylammonium lead tribromide perovskite single crystals to environmental gases. *Sci. Adv.* 2: e1600534 (1-10).

135 Zohar, A., Kedem, N., Levine, I. et al. (2016). Impedance spectroscopic indication for solid state electrochemical reaction in $(CH_3NH_3)PbI_3$ films. *J. Phys. Chem. Lett.* 7: 191–197.

136 Brenes, R., Guo, D., Osherov, A. et al. (2017). Metal halide perovskite polycrystalline films exhibiting properties of single crystals. *Joule* 1: 155–167.

137 Kong, W., Rahimi-Iman, A., Bi, G. et al. (2016). Oxygen intercalation induced by photocatalysis on the surface of hybrid lead halide perovskites. *J. Phys. Chem. C* 120: 7606–7611.

138 Aristidou, N., Sanchez-Molina, I., Chotchuangchutchaval, T. et al. (2015). The role of oxygen in the degradation of methylammonium lead trihalide perovskite photoactive layers. *Angew. Chem. Int. Ed.* 54: 8208–8212.

139 Pearson, A.J., Eperon, G.E., Hopkinson, P.E. et al. (2016). Oxygen degradation in mesoporous $Al_2O_3/CH_3NH_3PbI_{3-x}Cl_x$ perovskite solar cells: kinetics and mechanisms. *Adv. Energy Mater.* 6: 1600014 (1-10).

140 O'Mahony, F.T.F., Lee, Y.H., Jellett, C. et al. (2015). Improved environmental stability of organic lead trihalide perovskite-based photoactive-layers in the presence of mesoporous TiO_2. *J. Mater. Chem. A* 3: 7219–7223.

141 Leijtens, T., Eperon, G.E., Pathak, S. et al. (2013). Overcoming ultraviolet light instability of sensitized TiO_2 with meso-superstructured organometal tri-halide perovskite solar cells. *Nat. Commun.* 4: 2885 (1-8).

142 Lee, S.W., Kim, S., Bae, S. et al. (2016). UV degradation and recovery of perovskite solar cells. *Sci. Rep.* 6: 38150 (1-10).

143 Nie, W., Blancon, J.C., Neukirch, A.J. et al. (2016). Light-activated photocurrent degradation and self-healing in perovskite solar cells. *Nat. Commun.* 7: 11574 (1-9).

144 Bischak, C.G., Hetherington, C.L., Wu, H. et al. (2017). Origin of reversible photoinduced phase separation in hybrid perovskites. *Nano Lett.* 17: 1028–1033.

145 Brennan, M.C., Draguta, S., Kamat, P.V., and Kuno, M. (2018). Light-induced anion phase segregation in mixed halide perovskites. *ACS Energy Lett.* 3: 204–213.

146 Roose, B., Baena, J.P.C., Gödel, K.C. et al. (2016). Mesoporous SnO_2 electron selective contact enables UV-stable perovskite solar cells. *Nano Energy* 30: 517–522.

147 Zhao, P., Han, M., Yin, W. et al. (2018). Insulated interlayer for efficient and photostable electron-transport-layer-free perovskite solar cells. *ACS Appl. Mater. Interfaces* 10: 10132–10140.

148 Sun, Y., Fang, X., Ma, Z. et al. (2017). Enhanced UV-light stability of organometal halide perovskite solar cells with interface modification and a UV absorption layer. *J. Mater. Chem. C* 5: 8682–8687.

149 Hoke, E.T., Slotcavage, D.J., Dohner, E.R. et al. (2015). Reversible photo-induced trap formation in mixed-halide hybrid perovskites for photovoltaics. *Chem. Sci.* 6: 613–617.

150 Slotcavage, D.J., Karunadasa, H.I., and McGehee, M.D. (2016). Light-induced phase segregation in halide-perovskite absorbers. *ACS Energy Lett.* 1: 1199–1205.

151 Yun Jae, S., Seidel, J., Kim, J. et al. (2016). Critical role of grain boundaries for ion migration in formamidinium and methylammonium lead halide perovskite solar cells. *Adv. Energy Mater.* 6: 1600330 (1-8).

152 Jena, A.K., Numata, Y., Ikegami, M., and Miyasaka, T. (2018). Role of spiro-OMeTAD in performance deterioration of perovskite solar cells at high temperature and reuse of the perovskite films to avoid Pb-waste. *J. Mater. Chem. A* 6: 2219–2230.

153 Jena, A.K., Ikegami, M., and Miyasaka, T. (2017). Severe morphological deformation of spiro-OMeTAD in $(CH_3NH_3)PbI_3$ solar cells at high temperature. *ACS Energy Lett.* 2: 1760–1761.

154 Carrillo, J., Guerrero, A., Rahimnejad, S. et al. (2016). Ionic reactivity at contacts and aging of methylammonium lead triiodide perovskite solar cells. *Adv. Energy Mater.* 6: 1502246 (1-7).

155 Zhao, Y., Zhou, W., Tan, H. et al. (2017). Mobile-ion-induced degradation of organic hole-selective layers in perovskite solar cells. *J. Phys. Chem. C* 121: 14517–14523.

156 Das, C., Kot, M., Hellmann, T. et al. (2020). Atomic layer-deposited aluminum oxide hinders iodide migration and stabilizes perovskite solar cells. *Cell Rep. Phys. Sci.* 1: 100112.

157 Rakstys, K., Igci, C., and Nazeeruddin, M.K. (2019). Efficiency vs. stability: dopant-free hole transporting materials towards stabilized perovskite solar cells. *Chem. Sci.* 10: 6748–6769.

158 Yang, W.S., Park, B.W., Jung, E.H. et al. (2017). Iodide management in formamidinium-lead-halide–based perovskite layers for efficient solar cells. *Science* 356: 1376–1379.

159 Islam, M.B., Yanagida, M., Shirai, Y. et al. (2017). NiOx hole transport layer for perovskite solar cells with improved stability and reproducibility. *ACS Omega* 2: 2291–2299.

160 Boyd, C.C., Shallcross, R.C., Moot, T. et al. (2020). Overcoming redox reactions at perovskite nickel oxide interfaces to boost voltages in perovskite solar cells. *Joule* 4: 1–17.

161 Rao, H., Ye, S., Sun, W. et al. (2016). A 19.0% efficiency achieved in CuOx-based inverted $CH_3NH_3PbI_{3-x}Cl_x$ solar cells by an effective Cl doping method. *Nano Energy* 27: 51–57.

162 Sun, W., Li, Y., Ye, S. et al. (2016). High-performance inverted planar heterojunction perovskite solar cells based on a solution-processed CuOx hole transport layer. *Nanoscale* 8: 10806–10813.

163 Hossain, M.I., Alharbi, F.H., and Tabet, N. (2015). Copper oxide as inorganic hole transport material for lead halide perovskite based solar cells. *Solar Energy* 120: 370–380.

164 Christians, J.A., Fung, R.C.M., and Kamat, P.V. (2014). An inorganic hole conductor for organo-lead halide perovskite solar cells. Improved hole conductivity with copper iodide. *J. Am. Chem. Soc.* 136: 758–764.

165 Wang, H., Yu, Z., Lai, J. et al. (2018). One plus one greater than two: high-performance inverted planar perovskite solar cells based on a composite CuI/CuSCN hole-transporting layer. *J. Mater. Chem. A* 6: 21435–21444.

166 Ye, S., Rao, H., Zhao, Z. et al. (2017). A breakthrough efficiency of 19.9% obtained in inverted perovskite solar cells by using an efficient trap state passivator cu(thiourea)I. *J. Am. Chem. Soc.* 139: 7504–7512.

167 Madhavan, V.E., Zimmermann, I., Baloch, A.A.B. et al. (2019). CuSCN as hole transport material with 3D/2D perovskite solar cells. *ACS Appl. Energy Mater* 3: 114–121.

168 Zhang, H., Wang, H., Chen, W., and Jen, A.K.Y. (2017). $CuGaO_2$: a promising inorganic hole-transporting material for highly efficient and stable perovskite solar cells. *Adv. Mater.* 29: 1604984.

169 Zhang, H., Wang, H., Zhu, H. et al. (2018). Low-temperature solution-processed $CuCrO_2$ hole-transporting layer for efficient and photostable perovskite solar cells. *Adv. Energy Mater.* 8: 1702762.

170 Jiang, X., Yu, Z., Li, H.-B. et al. (2017). A solution-processable copper (II) phthalocyanine derivative as a dopant-free hole-transporting material for efficient and stable carbon counter electrode-based perovskite solar cells. *J. Mater. Chem. A.* 5: 17862–17866.

171 Yin, X., Song, Z., Li, Z., and Tang, W. (2020). Toward ideal hole transport materials: a review on recent progress in dopant-free hole transport materials

for efficient and stable perovskite solar cells. *Energy Environ. Sci.* https://doi.org/10.1039/D0EE02337J.

172 Huang, C., Fu, W., Li, C.Z. et al. (2016). Dopant-free hole-transporting material with a C3h symmetrical truxene core for highly efficient perovskite solar cells. *J. Am. Chem. Soc.* 138: 2528–2531.

173 Azmi, R., Nam, S.Y., Sinaga, S. et al. (2018). High-performance dopant-free conjugated small molecule-based hole-transport materials for perovskite solar cells. *Nano Energy* 44: 191–198.

174 Cao, Y., Li, Y., Morrissey, T. et al. (2019). Dopant-free molecular hole transport material that mediates a 20% power conversion efficiency in a perovskite solar cell. *Energy Environ. Sci.* 12: 3502–3507.

175 Paek, S., Qin, P., Lee, Y. et al. (2017). Dopant-free hole-transporting materials for stable and efficient perovskite solar cells. *Adv. Mater.* 29: 1606555.

176 Xu, P., Liu, P., Li, Y. et al. (2018). D–A–D-typed hole transport materials for efficient perovskite solar cells: tuning photovoltaic properties via the acceptor group. *ACS Appl. Mater. Interfaces* 10: 19697–19703.

177 Feng, Y., Hu, Q., Rezaee, E. et al. (2019). Perovskite solar cells: high performance and stable perovskite solar cells based on dopant-free arylamine-substituted copper (II) phthalocyanine hole-transporting materials. *Adv. Energy Mater.* 9: 1970104.

178 Duong, T., Peng, J., Walter, D. et al. (2018). Perovskite solar cells employing copper phthalocyanine hole-transport material with an efficiency over 20% and excellent thermal stability. *ACS Energy Lett.* 3 (10): 2441–2448.

179 Zhang, L., Liu, C., Zhang, J. et al. (2018). Intensive exposure of functional rings of a polymeric hole-transporting material enables efficient perovskite solar cells. *Adv. Mater.* 30: 1804028.

180 Kim, G.-W., Lee, J., Kang, G. et al. (2018). Donor–acceptor type dopant-free, polymeric hole transport material for planar perovskite solar cells (19.8%). *Adv. Energy Mater.* 8: 1701935.

181 Öz, S., Jena, A., Kulkarni, A. et al. (2020). Lead (II) propionate additive and a dopant-free polymer hole transport material for $CsPbI_2Br$ perovskite solar cells. *ACS Energy Lett.* 5: 1292–1299.

182 Eperon, G.E., Paterno, G.M., Sutton, R.J. et al. (2015). Inorganic caesium lead iodide perovskite solar cells. *J. Mater. Chem. A.* 3: 19688–19695.

183 Wang, Y., Dar, M.I., Ono, L.K. et al. (2019). Thermodynamically stabilized β-CsPbI3–based perovskite solar cells with efficiencies >18%. *Science* 365: 591–595.

184 Zhang, T., Dar, M.I., Li, G. et al. (2017). Bication lead iodide 2D perovskite component to stabilize inorganic α-$CsPbI_3$ perovskite phase for high-efficiency solar cells. *Sci. Adv.* 3: e1700841 (1-7).

185 Jena, A.K., Kulkarni, A., Sanehira, Y. et al. (2018). Stabilization of α-$CsPbI_3$ in ambient room temperature conditions by incorporating Eu into $CsPbI_3$. *Chem. Mater.* 30: 6668–6674.

186 Wang, P., Zhang, X., Zhou, Y. et al. (2018). Solvent-controlled growth of inorganic perovskite films in dry environment for efficient and stable solar cells. *Nat. Commun.* 9: 2225 (1-7).

187 Liu, C., Li, W., Zhang, C. et al. (2018). All-inorganic $CsPbI_2Br$ perovskite solar cells with high efficiency exceeding 13%. *J. Am. Chem. Soc.* 140: 3825–3828.

188 Babayigit, A., Ethirajan, A., Muller, M., and Conings, B. (2016). Toxicity of organometal halide perovskite solar cells. *Nat. Mater.* 15: 247–251.

189 Guo, Z., Jena, A.K., Takei, I. et al. (2021). Dopant-free polymer HTM-based $CsPbI_2Br$ Solar Cells with efficiency over 17% in sunlight and 34% in indoor light. *Adv. Func. Mat.* 31: 202103614R1.

190 Ke, W. and Kanatzidis, M.G. (2019). Prospects for low-toxicity lead-free perovskite solar cells. *Nat. Commun.* 10: 965.

191 Jokar, E., Chien, C.H., Tsai, C.M. et al. (2019). Robust tin-based perovskite solar cells with hybrid organic cations to attain efficiency approaching 10%. *Adv. Mater.* 31: 1804835.

192 Liu, X., Wang, Y., Wu, T. et al. (2020). Efficient and stable tin perovskite solar cells enabled by amorphous-polycrystalline structure. *Nat. Commun.* 11: 2678.

193 Tai, Q., Guo, X., Tang, G. et al. (2019). Antioxidant grain passivation for air-stable tin-based perovskite solar cells. *Angew. Chem.* 58: 806–810.

194 Kamarudin, M.A., Hirotani, D., Wang, Z. et al. (2019). Suppression of charge carrier recombination in lead-free tin halide perovskite via Lewis base post-treatment. *J. Phys. Chem. Lett.* 10 (17): 5277–5283.

195 Kawai, T., Ishii, A., Kitamura, T. et al. (1996). Optical absorption in band-edge region of $(CH_3NH_3)_3Bi_2I_9$ single crystals. *J. Phys. Soc. Jpn.* 65: 1464–1468.

196 Arakcheeva, A., Bonin, M., Chapuis, G., and Zaitsev, A.I. (1999). The phases of $Cs_3Bi_2I_9$ between RT and 190 K. *Z. Kristallogr. Cryst. Mater.* 214: 279–283.

197 Szklarz, P., Pietraszko, A., Jakubas, R. et al. (2008). Structure, phase transitions and molecular dynamics of $[C(NH_2)_3]_3[M_2I_9]$, M = Sb, Bi. *J. Phys. Condens. Matter* 20: 255221.

198 Kulkarni, A., Singh, T., Ikegami, M., and Miyasaka, T. (2017). Photovoltaic enhancement of bismuth halide hybrid perovskite by N-methyl pyrrolidone-assisted morphology conversion. *RSC Adv.* 7: 9456–9460.

199 Zhang, Z., Li, X., Xia, X. et al. (2017). High-quality $(CH_3NH_3)_3Bi_2I_9$ film-based solar cells: pushing efficiency up to 1.64%. *J. Phys. Chem. Lett.* 8 (17): 4300–4307.

200 Jain, S.M., Phuyal, D., Davies, M.L. et al. (2018). An effective approach of vapour assisted morphological tailoring for reducing metal defect sites in lead-free, $(CH_3NH_3)_3Bi_2I_9$ bismuth-based perovskite solar cells for improved performance and long-term stability. *Nano Energy* 49: 614–624.

201 Kim, Y., Yang, Z., Jain, A. et al. (2016). Pure cubic-phase hybrid iodobismuthates $AgBi_2I_7$ for thin-film photovoltaics. *Angew. Chem.* 128: 9738–9742.

202 Kulkarni, A., Jena, A.K., Ikegami, M., and Miyasaka, T. (2019). Performance enhancement of $AgBi_2I_7$ solar cells by modulating a solvent-mediated adduct

and tuning remnant BiI_3 in one-step crystallization. *Chem. Commun.* 55: 4031–4034.

203 Kim, H.D., Ohkita, H., Benten, H., and Ito, S. (2016). Photovoltaic performance of perovskite solar cells with different grain sizes. *Adv. Mater.* 28: 917–922.

204 Harikesh, P.C., Mulmudi, H.K., Ghosh, B. et al. (2016). Rb as an alternative cation for templating inorganic lead-free perovskites for solution processed photovoltaics. *Chem. Mater.* 28: 7496–7504.

205 Boopathi, K.M., Karuppuswamy, P., Singh, A. et al. (2017). Solution-processable antimony-based light-absorbing materials beyond lead halide perovskites. *J. Mater. Chem. A* 5: 20843–20850.

206 Jiang, F., Yang, D., Jiang, Y. et al. (2018). Chlorine-incorporation-induced formation of the layered phase for antimony-based lead-free perovskite solar cells. *J. Am. Chem. Soc.* 140: 1019–1027.

207 Nie, R., Mehta, A., Park, B.W. et al. (2018). Mixed sulfur and iodide-based lead-free perovskite solar cells. *J. Am. Chem. Soc.* 140: 872–875.

208 Chen, M., Ju, M.G., Carl, A.D. et al. (2018). Cesium titanium (IV) bromide thin films based stable lead-free perovskite solar cells. *Joule* 2: 558–570.

209 Debbichi, L., Lee, S., Cho, H. et al. (2018). Mixed valence perovskite $Cs_2Au_2I_6$: a potential material for thin-film Pb-free photovoltaic cells with ultrahigh efficiency. *Adv. Mater.* 30: 1707001.

210 Nie, R., Sumukam, R.R., Reddy, S.H. et al. (2020). Lead-free perovskite solar cells enabled by hetero-valent substitutes. *Energy Environ. Sci.* 13: 2363–2385.

211 Löper, P., Moon, S.J., Martín de Nicolas, S. et al. (2015). Organic–inorganic halide perovskite/crystalline silicon four-terminal tandem solar cells. *Phys. Chem. Chem. Phys.* 17: 1619–1629.

212 Jošt, M., Kegelmann, L., Korte, L., and Albrecht, S. (2020). Monolithic perovskite tandem solar cells: a review of the present status and advanced characterization methods toward 30% efficiency. *Adv. Energy Mater.* 10: 1904102.

213 Zhang, A., Li, Z., Meng, L. et al. (2020). Perovskite-based tandem solar cells: get the most out of the sun. *Adv. Funct. Mater.* 30: 2001904.

214 McMeekin, D.P., Sadoughi, G., Rehman, W. et al. (2016). A mixed-cation lead mixed-halide perovskite absorber for tandem solar cells. *Science* 351: 151–155.

215 Bush, K.A., Palmstrom, A.F., Yu, Z.J. et al. (2017). 23.6%-efficient monolithic perovskite/silicon tandem solar cells with improved stability. *Nat. Energy* 2: 17009.

216 Jäger, K., Kolte, L., Rech, B., and Albrecht, S. (2017). Numerical optical optimization of monolithic planar perovskite-silicon tandem solar cells with regular and inverted device architectures. *Opt. Express* 25: A473–A482.

217 Duong, T., Wu, Y., Shen, H. et al. (2017). Rubidium multication perovskite with optimized bandgap for perovskite-silicon tandem with over 26% efficiency. *Adv. Energy Mater.* 7: 1700228.

218 Yu, Z., Yang, Z., Ni, Z. et al. (2020). Simplified interconnection structure based on C60/SnO_{2-x} for all-perovskite tandem solar cells. *Nat. Energy* 5: 657–665.

219 Xiao, K., Lin, R., Han, O. et al. (2020). All-perovskite tandem solar cells with 24.2% certified efficiency and area over 1 cm^2 using surface-anchoring zwitterionic antioxidant. *Nat. Energy* 5: 870–880.

220 Moot, T., Werner, J., Eperon, G.E. et al. (2020). Choose your own adventure: fabrication of monolithic all-perovskite tandem photovoltaics. *Adv. Mater.* 32: 2003312, 1–22.

221 Lang, F., Nickel, N.H., Bundesmann, J. et al. (2016). Radiation hardness and self-healing of perovskite solar cells. *Adv. Mater.* 28: 8726–8731.

222 Miyazawa, Y., Kim, G.M., Ishii, A. et al. (2021). Evaluation of damage coefficient for minority-carrier diffusion length of triple-cation perovskite solar cells under 1 MeV electron irradiation for space applications. *J. Phys. Chem. C.* 125: 13131–13137.

223 Brus, V.V., Lang, F., Bundesmann, J. et al. (2017). Defect dynamics in proton irradiated $CH_3NH_3PbI_3$ perovskite solar cells. *Adv. Electron. Mater.* 3: 1600438.

224 Miyazawa, Y., Ikegami, M., Chen, H.W. et al. (2018). Tolerance of perovskite solar cell to high-energy particle irradiations in space environment. *iScience* 2: 148–155.

225 Lang, F., Jost, M., Frohna, K. et al. (2020). Proton radiation hardness of perovskite tandem photovoltaics. *Joule* 4: 1054–1069.

226 Reb, L.K., Böhmer, M., Predeschly, B. et al. (2020). Perovskite and organic solar cells on a rocket flight. *Joule* 4: 1880–1892.